Anat Sci Int (2017) 92:55–78
DOI 10.1007/s12565-016-0355-9

REVIEW ARTICLE

Renaissance of morphological studies: the examination of functional structures in living animal organs using the in vivo cryotechnique

Shinichi Ohno[1] · Yurika Saitoh[1] · Nobuhiko Ohno[1,3] · Nobuo Terada[1,2]

Received: 18 May 2016 / Accepted: 27 June 2016 / Published online: 18 July 2016

Abstract Medical and biological scientists wish to understand the in vivo structures of the cells and tissues that make up living animal organs, as well as the locations of their molecular components. Recently, the live imaging of animal cells and tissues with fluorescence-labeled proteins produced via gene manipulation has become increasingly common. Therefore, it is important to ensure that findings derived from histological or immunohistochemical tissue sections of living animal organs are compatible with those obtained from live images of the same organs, which can be assessed using recently developed digital imaging techniques. Over the past two decades, we have performed immunohistochemical and morphological studies of the cells and tissues in living animal organs using a novel in vivo cryotechnique. The use of a specially designed liquid cryogen system with or without a cryoknife during this cryotechnique solved the technical problems that inevitably arise during the conventional preparation methods employed prior to light or electron microscopic examinations. Our in vivo cryotechnique has been found to be extremely useful for arresting transient physiological processes in cells and tissues and for maintaining their functional components—such as rapidly changing signaling molecules, membrane channels, or receptors—in situ. The purpose of the present review is to describe the basic mechanism underlying cryotechniques and the significance of our in vivo cryotechnique. In addition, it describes various morphological or immunohistochemical findings, observations made using quantum dots, and a Raman cryomicroscopy-based method for assessing oxygen saturation in the erythrocytes flowing through intestinal tissues.

Keywords Bioimaging · Functional morphology · In vivo cryotechnique · Living animal organ · Soluble component

Introduction

Morphological studies involving light, electron, or scanning probe microscopy are the major approaches used to understand the physiological and pathological features of animal or human organs in the field of biomedicine. In particular, conventional electron microscopy, which was developed in the latter half of the twentieth century, has greatly facilitated ultrastructural analyses of cells and tissues. Although the research techniques used in molecular biology and genetics have progressed rapidly, leading to the establishment of new molecular and biological fields, morphological techniques are still required to obtain a more precise understanding of the cells and tissues found in animal and human organs. Such morphological findings also provide functional information about the target tissues/organs.

Shinichi Ohno: Retired at the end of March 2015, and is now an Emeritus Professor at the University of Yamanashi.

Yurika Saitoh: Moved to Teikyo University of Science in April 2016.

Nobuhiko Ohno: Moved to the National Institute for Physiological Science in April 2016.

✉ Shinichi Ohno
sohno@yamanashi.ac.jp

[1] Department of Anatomy and Molecular Histology, Interdisciplinary Graduate School of Medicine and Engineering, University of Yamanashi, Chuo, Japan

[2] Division of Health Sciences, Shinshu University Graduate School of Medicine, Matsumoto, Japan

[3] Division of Neurobiology and Bioinformatics, National Institute for Physiological Sciences, Okazaki, Japan

Chemical fixation and alcohol dehydration are both commonly used to prepare cells and tissues for routine morphological analyses; however, they always introduce numerous morphological artifacts, including tissue shrinkage, and result in the extraction of soluble components (Fig. 1a, b) (Furukawa et al. 1991; Yoshimura et al. 1991; Ohno et al. 1992). Quick freezing (QF) and high-pressure freezing methods, in which resected fresh organ tissues are quickly frozen for physical fixation, have contributed to reducing the frequency of such artifacts (Fig. 1c, d) (Yu et al. 1997, 1998). However, in these methods, tissue specimens have to be resected from the target organ together with a blood supply prior to the freezing procedure. Therefore, the tissue specimens are inevitably exposed to stress, such as ischemia and anoxia, and hence do not represent the normal morphological state of the target tissue.

The final goal of morphological and immunohistochemical studies in the field of biomedicine is to obtain findings in animal experiments or human clinical cases that accurately reflect the physiological or pathological functional state of the target tissue. Therefore, it is necessary to preserve all of the original components of the target cells/tissues in order to be able to describe the functional morphology of living animal or human organs. It is generally accepted that the morphological features of animal organs are modified when their blood supply is abrogated (because of ischemia or anoxia). Thus, there is a need to develop a new preparation technique for freezing living animal organs in vivo that makes it possible to accurately identify the morphology of the target tissue and to determine the immunolocalization of soluble components in functioning cells and tissues. In the last few decades, we have developed a novel "in vivo cryotechnique" (IVCT) that can be used to study dynamic changes in morphology and the immunolocalization of functioning soluble proteins in cells and tissues at the light or electron microscopic level (Fig. 1f), and to clarify the morphofunctional roles of the cells and tissues in living animal organs (Ohno et al. 1996, 2004, 2016).

Morphological problems associated with sample preparation and basic knowledge regarding the in vivo cryotechnique

Problems with conventional sample preparation techniques

In morphological studies of animal organs, the resected target tissues are subjected to various preparation

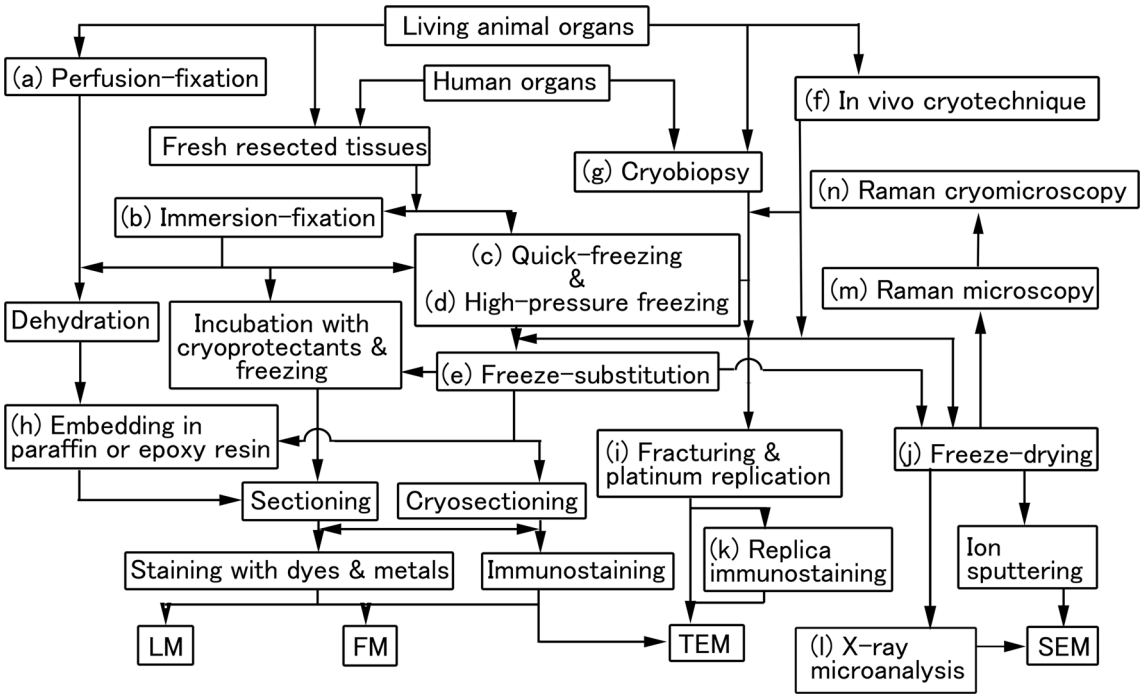

Fig. 1 A flowchart of the various procedures used to prepare tissue samples for light microscopy (*LM*), fluorescence microscopy (*FM*), transmission electron microscopy (*TEM*), or scanning electron microscopy (*SEM*). Perfusion (*a*) or immersion (*b*) fixation together with the associated dehydration techniques, quick freezing (*c*) and high-pressure freezing (*d*) methods, and the "in vivo cryotechnique" (*IVCT*) (*f*) are described. The subsequent preparatory steps are also shown. Note that all of the preparatory techniques used after the quick freezing (*c*) and high-pressure freezing (*d*) methods can also be employed after the IVCT (*f*). When applying the IVCT to human organs, the "cryobiopsy" technique (a new biopsy cryotechnique) (*g*) should be employed

procedures, including chemical fixation, alcohol dehydration, paraffin or epoxy resin embedding, sectioning, and/or dye or metal staining, before they are examined with a light or electron microscope (Fig. 1a, b, h). During these preparatory steps, various kinds of artifacts inevitably arise that modify the target tissue's morphology, especially during the conventional fixation and dehydration steps (Terada and Ohno 2004; Zea-Aragon et al. 2004a; Ohno et al. 2005). The fixation of tissue samples for light or electron microscopy is usually performed with common chemical fixatives, such as paraformaldehyde, glutaraldehyde, or osmium tetroxide. However, some technical problems have been reported to occur during chemical fixation (Terada and Ohno 2004). One such problem is that both molecular movement and structural changes can easily occur in cells and tissues during the fixation process. For example, soluble components such as proteins, lipids, and carbohydrates can easily be translocated within cells and tissues before the chemical-fixative-induced molecular crosslinking takes effect. Another problem is that dynamic morphological in vivo images of cells and tissues, such as images of muscle contraction and blood flow, are difficult to capture using conventional chemical fixation (Terada and Ohno 2004) because it takes time for the molecular crosslinking to occur.

Technical problems can also arise during the subsequent preparation steps, such as alcohol dehydration and routine embedding in paraffin wax or epoxy resin at high temperatures. Alcohol dehydration often leads to the shrinkage of resected tissue blocks. In addition, during the embedding of tissue samples in epoxy resin for electron microscopy, the initial polymerization step usually requires the samples to be heated to 35°, 45°, and 60 °C for 12 h each, which can have heat-related effects on the dehydrated biological specimens. Even during routine electron microscopic examinations, ultrathin sections that have been stained with uranium and/or lead have to be placed into vacuum chambers and can suffer heat-induced damage caused by the accelerating electron beams, which can reach temperatures of more than 100 °C. Although conventional tissue sample preparation techniques can cause several problems, many of the ultrastructural studies conducted in the twentieth century yielded important morphofunctional findings and contributed markedly to academic achievement in the biomedical field. However, morphologists have made a strong effort to avoid technical artifacts arising during the preparation of tissue samples for electron or light microscopy. Accordingly, the QF method was introduced in the middle of the twentieth century (Harreveld and Crowell 1964; Plattner and Bachmann 1982), and dramatic improvements in this method were made during the late twentieth century, resulting in the development of high-pressure freezing (Moor et al. 1980; Studer et al. 1989), which is especially important for electron microscopic studies.

Quick freezing (QF) method for resected fresh tissues

The QF method is a physical cryofixation technique in which resected biological animal organ specimens are quickly embedded in vitrified ice crystals as soon as possible rather than being chemically fixed (Fig. 1c). In the context of QF, cryotechniques, etc., the term "vitrification" usually refers to the formation of ice crystals that are not visible at the electron-microscopic level. The larger ice crystals that form at slower freezing speeds can often destroy the ultrastructures of cells and tissues. Resected fresh animal tissues that have not been treated with cryoprotectants should be frozen at a very high cooling rate (usually more than 10^5 °C/s) or under very high pressure (a few thousand times higher than atmospheric pressure). Over the last few decades, various QF methods have been developed. In the "slamming QF" method, resected fresh animal tissues are slammed onto copper blocks that have been cooled in liquid helium (−269 °C) or liquid nitrogen (−196 °C). On the other hand, the "plunging QF" method involves the samples being plunged into a liquid cryogen, such as propane or an isopentane/propane (IP) mixture (−193 °C) that has been cooled in liquid nitrogen. In these two QF methods, no detectable ice crystals form in the tissue located <10 μm below the surface that comes into contact with the cooled copper or cryogen. On the other hand, high-pressure freezing is a little different from QF (Fig. 1d) because it is performed under very high pressure to ensure that vitrification occurs within relatively broad areas of tissue.

Tissue samples that have been subjected to QF or high-pressure freezing might subsequently undergo various preparatory procedures. One of them is the freeze-substitution (FS) fixation method (Fig. 1e), in which the frozen specimens are usually incubated in cooled organic solvents containing chemical fixatives such as osmium tetroxide, glutaraldehyde, or paraformaldehyde at about −80 °C (van Harreveld and Trubatch 1975; Jehl et al. 1981; Cole et al. 1990). After being subjected to FS fixation, they are often embedded in epoxy resin, paraffin wax, or other hydrophilic materials to prepare them for the subsequent polymerization and sectioning steps (Fig. 1h). However, FS-treated specimens are known to be affected to some extent by the organic solvents and chemical fixatives used during the substitution process. To solve this problem, a deep-etching (DE) replication method has been developed in which replicas of the membranes of freeze-fractured and deeply etched tissues are obtained by subjecting the tissues to rotary shadowing with platinum and carbon at

temperatures below −100 °C under high vacuum conditions (Fig. 1i). The QF-DE method is considered to be useful for preventing the ultrastructural artifacts induced by the organic solvents used in the FS method.

As described above, one of the advantages of the QF and high-pressure freezing methods is that they result in better preservation of intra- and extracellular materials and cause fewer morphological artifacts (Yoshimura et al. 1991; Ohno et al. 1992; Yu et al. 1997, 1998). As a result, these methods have often been used to obtain ultrastructural findings over the past few decades. However, regardless of the cryotechniques employed for physical cryofixation, pieces of tissue always have to be resected and removed from the target living animal organ prior to the freezing process. It has been pointed out that the morphology of such tissue samples inevitably changes during these preparatory steps because of the effects of ischemia and anoxia. Thus, the QF and high-pressure freezing methods have rarely been used to examine the dynamic changes in the morphology of living animal organs, which are affected by blood pressure (Ohno et al. 1996, 2004). Furthermore, immunohistochemical analyses of the changes in receptors, membrane channels, or signaling molecules would be difficult to perform in specimens that have been prepared using conventional cryotechniques. To overcome these technical issues, it is necessary to avoid tissue resection and to directly freeze the target tissue in vivo under normal blood circulation conditions. Although a few pioneering studies have employed cryotechniques in order to solve the technical problems associated with ischemia and anoxia, the establishment of novel cryotechniques proved difficult until the development of our IVCT, which consistently and accurately captures the in vivo morphology of living animal organs (Ohno et al. 1996).

Development of the in vivo cryotechnique (IVCT)

The IVCT, which was developed between 1994 and 1996, is an original technique for directly cryofixing living animal organs without separating them from their blood supply (Fig. 1f) (Ohno et al. 1996). Briefly, after the target organ is exposed under anesthesia, it is quickly cut with a cryoknife that has been precooled in liquid nitrogen (−196 °C), and an IP mixture (−193 °C) is simultaneously poured over it, followed by liquid nitrogen, using a newly developed "in vivo cryoapparatus" (Ohno et al. 2004). By using a combination of a cryoknife and a liquid cryogen, good vitrification of the frozen in vivo tissue can be obtained at the electron microscopic level to a depth of several micrometers below the cryocut tissue surface (Ohno et al. 1996). In addition, at the light microscopic level, the tissue areas without detectable ice crystals extend for more than a few hundred micrometers below the cryocut tissue surface because the spatial resolution of light microscopes is much too low to detect the tiny ice crystals that arise in cells or tissues during rapid freezing (Terada and Ohno 2004; Ohno et al. 2005). The most significant advantage of the IVCT is that the normal blood supply of the target animal organ is strictly preserved at the moment of freezing. So, it becomes possible to immediately cryofix the cells and tissues of living animal organs while reducing the number of technical artifacts caused by ischemia or anoxia. Therefore, it is now possible to examine the extra- and intracellular structures and molecular distributions of animal tissues in the dynamic (i.e., living) state, which have proven difficult to detect using other conventional cryotechniques.

The IVCT method

The IVCT has been performed with an in vivo cryoapparatus (described in the next paragraph) since the year 2000. In the original IVCT, which was developed between 1994 and 1996 and carried out by a team of three operators, the IP cryogen (−193 °C) was manually poured over the exposed target organ, which was simultaneously cryocut with a precooled cryoknife in liquid nitrogen (−196 °C) (Ohno et al. 1996). After the IP cryogen had been poured over the target animal organ for several seconds, the process was repeated with liquid nitrogen, and then the frozen organs were broken off from the rest of the animal's body and plunged into liquid nitrogen for preservation. Thereafter, frozen tissue samples were collected from the target organ using a dental electric drill in liquid nitrogen. However, it is difficult for a single operator to manually perform all of the preparatory procedures and to consistently obtain well-frozen tissue specimens. To facilitate the IVCT, the in vivo cryoapparatus (EIKO Corporation, Hitachinaka, Ibaraki, Japan) was developed (Ohno et al. 2004; Zea-Aragon et al. 2004a). The manual operation of the in vivo cryoapparatus" will be described in the next paragraph. After the IVCT has been performed and frozen tissue samples have been removed from the target organ, various preparation steps are employed prior to the morphological analysis (Fig. 1e, i, j, m, n).

Practical procedures associated with the use of the in vivo cryoapparatus

The IVCT was originally performed with a handmade in vivo cryoapparatus by a team of three operators, as described in detail in a previous study (Ohno et al. 1996). The manual operation of the in vivo cryoapparatus is briefly described in this paragraph. Step 1: Pour some liquid nitrogen into two reservoirs to cool them down. Once the cooling of the reservoirs has started, it is

important that they are continuously cooled with liquid nitrogen. If they are temporarily warmed up, the water produced by the melting of the attached frost will completely cover the valves of the cryoapparatus. Then, when the reservoirs are cooled down again to a temperature below 0 °C, the valves will become completely frozen and immobilized. Step 2: Set the timer for the controller and press the foot switch to check whether the liquid nitrogen in the reservoirs is able to pass through the nozzles as planned. This step is important for preventing accidents associated with the cryoapparatus. Step 3: Pour the IP cryogen into the reservoir. The cryogen is prepared beforehand by bubbling propane gas through liquid isopentane that has been precooled in liquid nitrogen and constantly agitated with a magnetic stirrer. The ratio of isopentane to propane should be 1:2–1:3 to achieve maximal cooling at about −193 °C (Jehl et al. 1981). Step 4: Expose the target organ under anesthesia. Step 5: Set the timer of the controller, and precool the cryoknife in liquid nitrogen in another container. A piece of sponge is sometimes attached to the cryoknife to absorb some liquid nitrogen and keep the cryoknife cool during its transfer over the exposed organ. Step 6: Bring the cooled cryoknife onto the exposed target organ and press the foot switch. Immediately after pressing the foot switch, cryocut the target organ manually with the cryoknife and then pour the IP cryogen through the nozzle, which is initiated by pressing the foot switch and is automatically regulated by the controller. Several seconds after the IP cryogen has been poured over the target organ, liquid nitrogen automatically pours onto the frozen organ through another nozzle. Step 7: Put the whole of the frozen organ in liquid nitrogen to preserve it until its removal. Step 8: Extract the target tissue from the frozen organ in the liquid nitrogen using a electric dental drill. After performing the IVCT and then removing the frozen tissue samples, various preparatory steps are employed prior to the morphological analysis (Fig. 1e, i, j, m, n).

Simple manual IVCT for light microscopy

When the IVCT is used to obtain samples for light microscopic observations, it can be performed more simply without a special cryoapparatus (Fig. 2) (Zhou et al. 2007; Terada et al. 2007a, b). In such cases, achieving a freezing temperature without any visible ice crystal formation is not always necessary for morphological examinations because of the lower spatial resolution of light microscopy. Instead, in vivo freezing can be performed by simply pouring the IP cryogen (−193 °C) directly onto the target organ (Fig. 2) (Zhou et al. 2007; Terada et al. 2007a). A pouring time of several seconds should be sufficient to obtain well-frozen cells and tissues because the cooling speed of the cryogen is much faster than that of liquid nitrogen alone. This simple cryoprocedure makes it easier to perform the IVCT when obtaining tissue samples for examinations at the light microscopic level. In the light microscopic specimens prepared in this manner, good morphological preservation can be achieved to a depth of a few hundred micrometers or less from the frozen surface. To analyze deeper areas of frozen tissue, the target living animal organ should be cut with a cryoknife that has been precooled in liquid nitrogen (Ohno et al. 1996), as described above, instead of manually pouring the liquid IP cryogen.

Preparation of the isopentane–propane (IP) cryogen

Step 1: Hang a 50-ml glass beaker containing a magnetic stirring bar in a Styrofoam box by wrapping it in steel wire (leaving steel wire handles on either side of the beaker) (Fig. 3a). Step 2: Place the box on a magnetic stirrer and check that the stirring bar in the beaker can be rotated. Step 3: Remove the beaker from the box and pour an appropriate amount of liquid nitrogen into the box so that it will be filled with liquid nitrogen when the beaker is placed back in the box (Fig. 3b). Step 4: Pour 15 ml of liquid isopentane into the beaker at room temperature. Hang the beaker in the box containing the liquid nitrogen and stir the isopentane. The liquid nitrogen will initially exhibit marked bubbling, but this will subside as the isopentane cools. Step 5: When the peripheral part of the isopentane has cooled to a similar temperature to the liquid nitrogen (−196 °C) and has begun to solidify, immediately place the tip of the nozzle of the propane gas tank into the cooled isopentane (Fig. 3c) and vigorously blow propane gas into

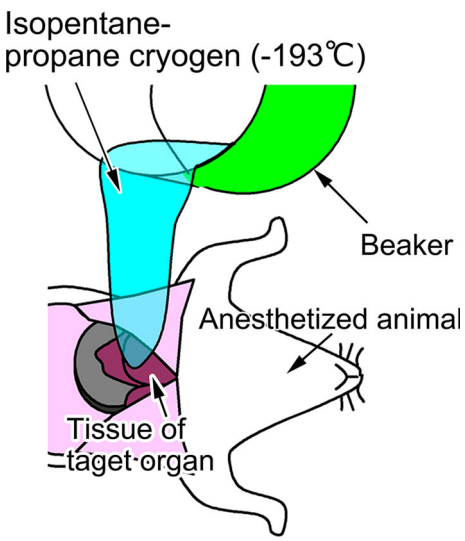

Fig. 2 Simple manual IVCT for light microscopy. In this method, isopentane–propane (IP) (the cryogen) (−193 °C) is directly poured over the target organs of anesthetized animals

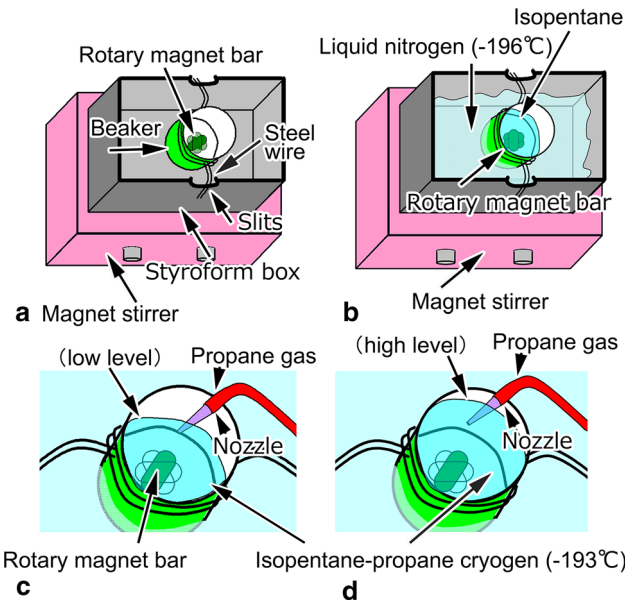

Fig. 3a–d Schematic drawings showing how the isopentane–propane (IP) cryogen can be prepared in a homemade plunge-freeze apparatus. **a** A *Styrofoam box* is shown. A wire is wrapped around a 50-ml beaker, and the box has slits for holding the ends of the wire. The beaker contains a magnetic stirring bar and is hung in the *Styrofoam box* above a *magnet stirrer* so that the *stirring bar* can rotate smoothly in the beaker. **b** Liquid nitrogen (−196 °C) is poured into the box. The beaker contains about 15 ml of liquid isopentane, which is continuously stirred with the stirring bar. When the bottom of the beaker is submerged in the liquid nitrogen, the liquid nitrogen immediately begins to bubble. **c** Propane gas is continuously released into the cooled isopentane, where it quickly liquefies, and the volume of the IP cryogen gradually rises. **d** When the volume of the liquid IP cryogen (−193 °C) reaches about 45 ml, the propane gas supply is cut off

the cooled isopentane to liquefy the propane gas. Step 6: Once the level of the IP cryogen in the beaker has reached about 45 ml (Fig. 3d), i.e., a ratio of isopentane to propane of 1:2–1:3, immediately cut off the propane gas supply. Step 7: Cover the Styrofoam box to minimize the extent to which the prepared IP cryogen is exposed to humid air.

Technical advantages of the IVCT

The main purpose of the IVCT is to rapidly freeze all of the biological components of the cells and tissues that make up the target living organ (Ohno et al. 1996, 2016). However, the required freezing time varies according to the depth of the target tissue from the frozen surface because the thermal conductance of cooling within cells/tissues depends on the continuous movement of thermal energy. Therefore, only tissue layers located at depths of about 10 and ≤200 μm freeze sufficiently to prevent the formation of visible ice crystals at the electron and light microscopic levels, respectively (Ohno et al. 1996, 2016). Each layer of frozen tissue is frozen at approximately the same time. Therefore, by routinely cutting epoxy resin or paraffin blocks almost parallel to the tissue surface using an ultramicrotome or a microtome, it is possible to obtain similarly frozen tissue specimens that cover wide areas of living animal organs.

Obtaining such tissue specimens using the QF method would require considerable amounts of liquid nitrogen (to plunge the fresh resected tissue samples into the cryogen or slam them onto copper metal blocks that have been precooled in liquid nitrogen). In the metal contact freezing method, the tissue samples are slightly compressed by the cooled copper metal during the impact (van Harreveld and Trubatch 1975), even though spacers and cushions are always inserted between the specimens and the cooled metal block. Conversely, when a liquid cryogen, such as an IP mixture that has been precooled in liquid nitrogen (Cole et al. 1990; Ohno et al. 1996; Zhou et al. 2007; Terada et al. 2007a), is used, the frozen tissue retains its original morphological state and does not suffer mechanical compression damage. This efficacy of liquid cryogen-based methods was confirmed in an experimental system in which human blood samples were sprayed into a liquid cryogen, which is referred to as the "in vitro cryotechnique for erythrocytes" and has been used to examine the dynamic changes in erythrocyte shape that occur at different blood flow speeds (Terada and Ohno 1998; Terada et al. 1998a).

To examine deeper tissue areas, it is necessary to cryocut the target organs under anesthesia (Ohno et al. 1996). When a cryoknife that has been precooled in liquid nitrogen passes through a living tissue, the part of the exposed tissue surface that comes into direct contact with the cryoknife is frozen in the same way as occurs during the metal contact method (Ohno et al. 1996). Mechanical damage is rarely seen in cryocut tissues providing that the cryoknife passes quickly through the target organ. The rest of the cryocut tissue is frozen by simultaneously pouring an IP mixture over it. During this process, the speed of the cryoknife movements and the freezing intensity of the cryogen are critical determinants of the time required to freeze the target tissue. Practically, at the electron microscopic level, well-frozen tissue is only seen within a very narrow band; i.e., the tissue located <10 μm below the frozen surface (Ohno et al. 1996). Although the thermal conductivity of living animal tissues gradually changes depending on the concentrations of biological materials, well-frozen tissue areas are sometimes seen next to damaged regions containing larger ice crystals despite both regions being located at the same distance from the frozen tissue surface, probably because of differences in the concentrations of soluble components among various cells and tissues.

The freeze-substitution (FS) fixation method

The FS fixation method is a commonly used technique in which ice crystals are replaced with an organic solvent containing fixatives and frozen tissue samples are embedded in synthetic resin or paraffin, which enables the functional morphology of cells and tissues at the time they were frozen to be visualized (Fig. 4b, e). During FS fixation, the frozen tissues—which contain a lot of liquid in vivo—in the organic solvent and fixatives are maintained below the freezing point because the ice crystals within them melt in the organic solvent during the incubation period. As a result, they are kept in their native state; i.e., their components are retained within the amorphous ice, and bridges simultaneously form between their components via chemical reactions with the fixatives during the FS process. To immunostain such tissue specimens, paraformaldehyde or glutaraldehyde is usually added to the organic acetone solvent. Using this FS method, the in vivo cell and tissue structures that exist at the time of freezing can be well preserved (Fig. 4b–d), and the findings of such specimens can be compared with those obtained during routine chemical fixation at room temperature, which allows the artificial modifications that occur during the latter process to be elucidated (Fig. 4a).

Benefits of FS fixation

During the QF of fresh resected tissues using the standard method (Fig. 4b), only the structures of the outer tissue layers are well frozen. This is because ice crystals form readily in animal organs during low-speed freezing. Therefore, the deep tissue regions that are poorly preserved in slow-freezing conditions should be carefully identified using hematoxylin and eosin (HE)-stained paraffin tissue sections. In such areas, the size of the ice crystals gradually increases from the well-frozen areas to the poorly frozen areas. In actively replicating cells that exhibit little chromatin condensation, more ice crystals appear to form in the nucleoplasm than in the cytoplasm. Moreover, it is considered that the water contents of cells and tissues at well-frozen sites are stored as tiny pieces of amorphous ice, which helps to preserve intermolecular gaps. This facilitates the penetration of antibodies and probes during immunostaining (Fig. 5b). When an organic acetone solvent is used for FS, it is important to consider whether it is necessary to use other factors to improve antibody or probe penetration, because the use of such solvents can lead to lipid extraction from intracellular membranous systems (Fig. 5), including cell membranes or double nuclear membranes. During the QF of fresh excised tissues, anoxia and ischemia promote the rapid extraction and continued movement of soluble proteins (Fig. 4b). Conversely, the IVCT with FS fixation method preserves the soluble proteins found in the cells and tissues of living animal organs (Figs. 4c, d, 5). As described above, the FS fixation method can maximize the benefits of various cryotechniques which are able to preserve cellular components in amorphous ice (Figs. 4, 5).

Practical FS fixation procedures for immunostaining

As stated above, FS fixation is a very useful fixation procedure for living animal tissue samples. In this section, practical FS procedures will be described in detail. Organic acetone solvent containing 2 % paraformaldehyde is

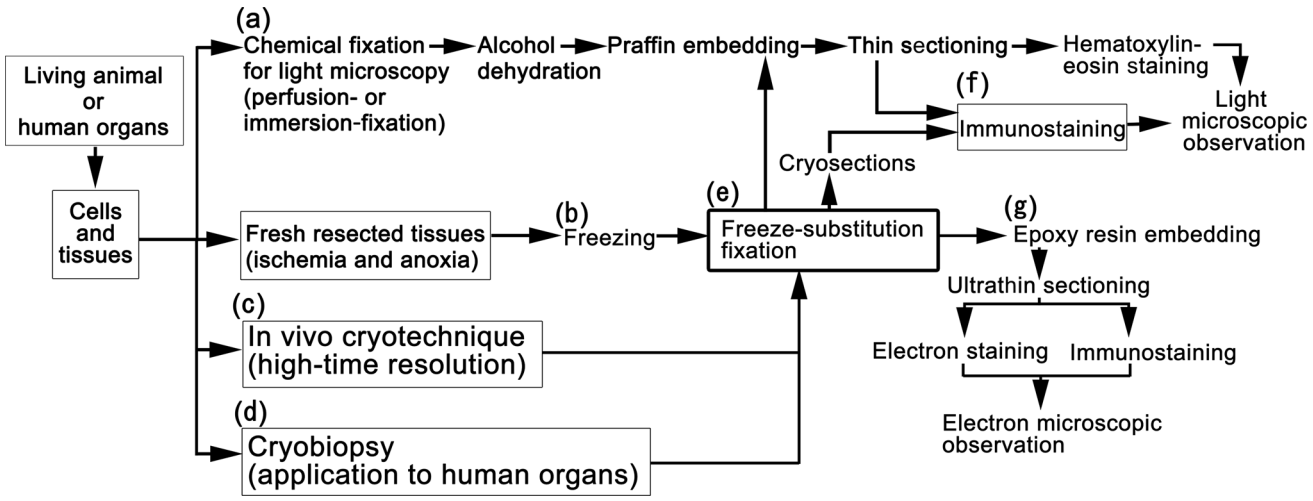

Fig. 4 A flowchart showing a series of conventional preparation procedures (*a*), quick freezing (*b*), the in vivo cryotechnique (*c*), and cryobiopsy (*d*). These procedures can be followed by freeze substitution (*e*) and immunostaining (*f*) or immunoelectron microscopy (*g*) in order to prepare tissue specimens for light or electron microscopic examinations

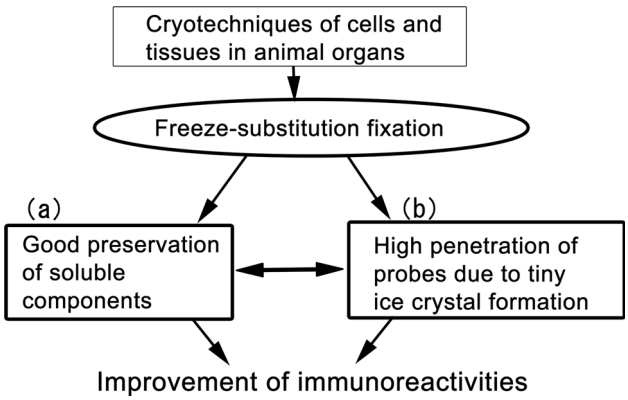

Fig. 5 Some of the technical advantages of using cryotechniques followed by freeze-substitution fixation for immunostaining. This technique has advantages for molecular preservation (*a*) and probe penetration (*b*)

usually used as the FS solution when preparing samples for light microscopy. In this method, the paraformaldehyde powder is first diluted to a concentration of 20 % in water before being added to acetone using a standard molecular sieve to completely remove any residual water. Although solid osmium tetroxide crystals are directly dissolved in acetone prior to conventional electron microscopy-based morphological examinations, both glutaraldehyde and paraformaldehyde are usually diluted in acetone prior to immunostaining at the light microscopic level after the preparation of solutions with higher concentrations. The stored frozen tissue samples are taken out of the liquid nitrogen (−196 °C) and placed into the FS solution in a container with a capacity of about 5 ml that has been cooled with dry ice acetone (about −80 °C). It can then be sealed at the same temperature as the dry ice acetone. Before moving the frozen samples into the FS solution, it is important to loosen the lid of the container, which can then be dipped in liquid nitrogen. Although the liquid nitrogen boils at first, this soon subsides, and the FS solution in the container begins to freeze from the portion that is in contact with the container wall. Then the container lid is opened, and the frozen tissue samples are transferred into the container. Finally, the container lid is tightly closed again and the container is returned to the dry ice acetone and kept at about −80 °C. FS fixation takes approximately 20–40 h in dry ice acetone kept at about −80 °C. The sample container is gradually returned to room temperature after the FS fixation. After slightly loosening the lid of the container, the tissue samples are kept in a refrigerator at a temperature of −20 °C for about 2 h and then transferred to another refrigerator compartment maintained at a temperature of 4 °C. After about 2 h, they are taken out of the refrigerator and left at room temperature. To prepare FS-fixed samples for light microscopic examinations, the tissue samples are lightly washed with pure acetone three times and embedded in paraffin wax after being passed through xylene. On the other hand, they are sometimes embedded in hydrophilic synthetic resin prior to electron microscopic immunostaining examinations.

Light microscopic immunostaining of FS-fixed tissues

In this section, we describe how freeze-substituted tissue samples should be prepared for light microscopic immunostaining. This method involves two different procedures. First, the samples are washed with pure acetone before being directly immersed in 20–30 % sucrose or glycerin solution (Fig. 4e). Then they are embedded in OCT compound, and cryosections are prepared in a cryostat (Fig. 4f). In such cases, because thick sections are required for immunostaining with fluorescence-labeled antibodies, we usually examine such sections using a confocal laser scanning microscope. The immunostaining of multiple molecules can be achieved by using a number of secondary antibodies with different fluorescent wavelengths. Furthermore, a fluorescent probe can be directly injected into the blood vessels of living animals, and the IVCT can be performed in combination with FS fixation to produce cryosections. To obtain paraffin-embedded sections, FS samples can be washed in pure acetone and xylene (Fig. 4e) and then routinely embedded in paraffin wax. This method makes permanent sample preparation possible, which is not the case when frozen cryosections are obtained, as described above. In addition, it is possible to prepare serial 4-μm-thick HE-stained sections for immunoperoxidase or immunofluorescent staining with various antibodies (Fig. 4f). Electron microscopic immunohistochemistry can be also performed (Fig. 4g).

Significance of ice crystal formation

As described in the previous sections, ice crystal formation is an inevitable problem during the use of cryotechniques, especially during sample preparation for electron microscopic examinations. However, ice crystal formation can sometimes aid immunohistochemistry at a light microscopic level (Terada and Ohno 2004; Ohno et al. 2005). During light microscopic immunohistochemistry, the immunoreactivity of many antigens is increased by ice crystal formation in animal tissues because it facilitates antibody and probe penetration (Fig. 5b) (Terada and Ohno 2004; Ohno et al. 2005). It was previously reported that cryotechniques are useful for immunostaining whole-mount mouse cerebellar samples (Bohrer et al. 1977). In an immunohistochemical study of the localization of soluble sphingosine kinase in mouse cerebellar tissue, soluble sphingosine kinase was found to exhibit a striped

immunolocalization pattern in the cerebellar layer on cryosections (Terada et al. 2004). Therefore, standard QF of the chemically fixed cerebellum followed by whole-mount organ immunostaining, which was aided by the formation of tiny ice crystals, was shown to be useful for revealing the marked compartmentalization of sphingosine kinase in the mouse cerebellum (Terada et al. 2004). Cryotechniques have also been employed during the intranuclear immunostaining of soluble signaling molecules in the living mouse cerebellum (Ohno et al. 2005). It is difficult to detect such intranuclear soluble antigens because of the presence of double nuclear membranes and compact materials composed of various proteins and nucleic acids as well as the delicate nature of the nucleoskeleton. However, the use of cryotechniques, especially the IVCT followed by FS fixation, has made it possible to clearly immunostain certain intranuclear signaling molecules, such as pCREB, in conventional paraffin sections without having to perform any antigen retrieval processes (Ohno et al. 2005). The improvement in the immunoreactivity of soluble signaling molecules brought about by ice crystal formation is extremely important because the existence of immunopositive target cells can only be determined based on the detection of immunoreactive products (Fig. 5a). If target cells and tissues are not clearly immunostained by specific antibodies then their in vivo biological functions and processes might be misunderstood. Thus, the effective ice crystal formation induced by cryotechniques should be kept in mind in cases in which immunohistochemical improvements are required (Terada and Ohno 2004; Terada et al. 2004; Ohno et al. 2005).

Biomedical applications of the IVCT

Renal glomeruli under various hemodynamic conditions

The renal glomerulus consists of intricate networks of blood capillaries in vivo, through which blood circulates under the influence of blood pressure. It is well known that hemodynamic factors, including the volume of renal blood, exert an important influence on glomerular functions and structures (Griffith et al. 1967; Kanwar 1984; Kriz et al. 1994). Therefore, alterations in the glomerular hemodynamics of renal corpuscles probably affect the driving mechanical force that modulates the permeability of glomerular filtration barriers (Ryan et al. 1976; Bohrer et al. 1977; Brenner et al. 1977; Kriz et al. 1994). For example, the distribution of serum albumin proteins in experimental rat glomeruli was reported to change in a hemodynamic condition-dependent manner (Ryan and Karnovsky 1976; Olivetti et al. 1981). Normal blood circulation therefore plays an important functional role in the maintenance of glomerular barrier function. In a previous scanning electron microscopic (SEM) study, we described the three-dimensional in vivo ultrastructures of functioning kidneys, which were prepared using the IVCT, under various hemodynamic conditions (Ohno et al. 2001).

Preparation procedures for SEM examinations of living mouse kidneys

The left kidneys of anesthetized mice were prepared under normal blood circulation conditions using the IVCT, as described previously (Ohno et al. 1996, 2001). Other mouse kidneys were prepared in a similar way after inducing cardiac arrest with an overdose of anesthetic to stop the blood supply to the kidneys or after ligating the lower abdominal aorta to acutely increase the blood supply to the kidneys. The IVCT-prepared specimens were routinely freeze-substituted in absolute acetone containing 2 % osmium tetroxide, before being transferred into *t*-butyl alcohol and then freeze-dried at −5 °C in a Hitachi ES-2030 apparatus. They were then mounted on aluminum stages, evaporated with platinum/palladium (10–15 nm) in a Hitachi E-1030 apparatus, and examined using a Hitachi S-4500 scanning electron microscope at an accelerating voltage of 5 kV.

Functioning podocytes under hemodynamic conditions

After the preparation of podocytes using the IVCT, many interdigitating foot processes, which covered the outer capillary surfaces of the renal corpuscles, were seen during normal blood circulation (Fig. 6a), and these findings were considered to reflect the in vivo structure of podocytes. The foot processes of the podocytes ran almost parallel to each other, and open filtration slits were seen at irregular intervals in some sections (Fig. 6b). Moreover, other foot processes with slits extended along the capillary loops (Fig. 6c), as was seen in freeze-fractured capillary loops. On the other hand, after cardiac arrest was induced, the urinary spaces collapsed (Fig. 6d), and the glomerular foot processes tightly adhered to each other (Fig. 6e). The foot processes were longer after cardiac arrest, as was seen in freeze-fractured capillary loops (Fig. 6e). In addition, stretched capillary loops were noted after the ligation of the aorta (Fig. 6f). Compared with the capillary loops seen after cardiac arrest (Fig. 6d, e), the interdigitating foot processes had wider filtration slits and were more loosely arranged after the ligation of the aorta (Fig. 6f). In a freeze-fractured renal corpuscle, urinary Bowman's spaces and the lumens of the capillary loops were more widely dilated (Fig. 6g), and several blood cells were found in the capillary lumens.

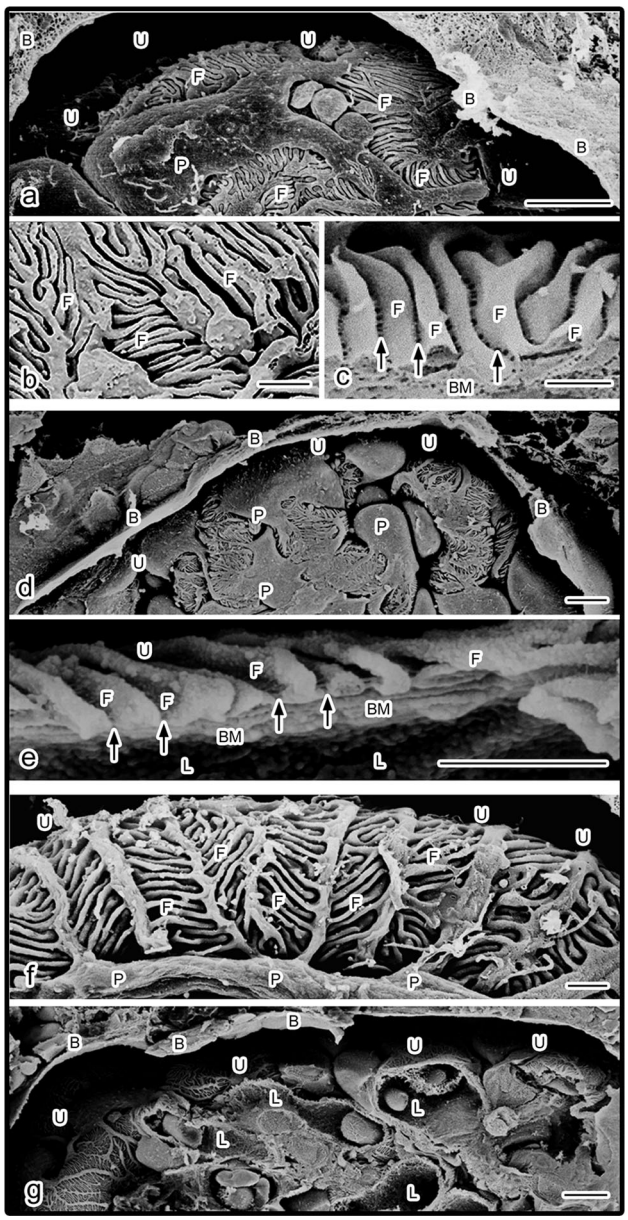

Fig. 6a–g Scanning electron micrographs of the freeze-fractured renal corpuscles of living mice obtained under normal blood flow (**a**–**c**), cardiac arrest (**d**, **e**), and aortic ligation (**f**, **g**) conditions using the IVCT. **a** Interdigitating foot processes covered the outer surfaces of the capillary loops. *P* podocyte, *F* foot process, *U* urinary space, *B* Bowman's capsule; *bar* 5 μm. **b** At higher magnification, the surface contours of the foot processes (*F*), which exhibited slits of various sizes, ran almost parallel to each other. *Bar* 1 μm. **c** Open filtration slits (*arrows*) were also seen between the foot processes (*F*) under the normal blood flow conditions. *BM* basement membrane; *bar* 0.5 μm. **d** A urinary space (*U*) that had almost collapsed and was covered by a Bowman's capsule (*B*) is shown. *Bar* 5 μm. **e** A freeze-fractured capillary loop is shown. Foot processes (*F*) with narrow filtration slits (*arrows*) were attached to the basement membrane (*BM*). *Bars* 1 μm; *L* capillary lumen, *U* urinary space. **f** Extended, thin interdigitating foot processes (*F*) covered the outer surfaces of the blood capillary loops. *P* podocyte, *U* urinary space; *bars* 1 μm. **g** The lumens of the freeze-fractured capillary loops (*L*) were wider, and dilation of the urinary space was also seen (*U*). *B* Bowman's capsule; *bar* 5 μm

Significance of foot processes for filtration

The glomerular capillary loops of living mouse kidneys are perpetually stretched by the hydraulic pressure in blood capillaries, whereas those in excised kidneys are not subjected to such stretching forces. The filtration slits between the foot processes of podocytes were reported to open widely to facilitate the passage of the glomerular filtrate in vivo (Kriz et al. 1994). It has also been reported that the foot processes are rich in contractile proteins such as actin, myosin, and α-actinin, and are capable of actin-mediated movement (Andrews 1988). Through this active movement, podocytes might regulate the glomerular filtration rate and thereby influence the hydraulic pressure across the glomerular basement membrane, as reported previously (Kriz et al. 1994). Therefore, blood pressure must be maintained at a stable level at the time of the IVCT, and the filtration slits found under normal blood circulation conditions are wider than those seen after the induction of cardiac arrest. Glomerular hydraulic pressure might be partially regulated by the relative width of the filtration slits. Thus, the width of the filtration slits is considered to play an important role in controlling hydraulic conductivity and water flow (Kriz et al. 1994; Drumond and Deen 1994). In a previous study, we obtained definitive morphofunctional confirmation of the living state of functioning mouse glomerular capillary loops, which indicated that the passage of solutes is affected by glomerular hemodynamics under different blood flow conditions (Ohno et al. 2001).

Pulmonary alveoli under respiratory conditions

Although some ultrastructural features of animal lungs were described in previous reports (Bastacky et al. 1995; Ham and Cormack 1978), these studies could not provide enough information about the physiological functions of the lungs in living animals. This is because conventional electron microscopy is not able to reveal the pulmonary ultrastructures of living animals during functional respiration. The fixation procedures employed during such examinations usually take several minutes, so it is hard to detect rapidly changing cellular events such as those that occur within a few milliseconds. Thus, conventional morphological studies have certain drawbacks that make them unsuitable for investigating the dynamic changes that take place in the lungs in vivo. The ultrastructure of the lung has been examined previously (Ham and Cormack 1978), but the authors of the latter study were unable to determine its

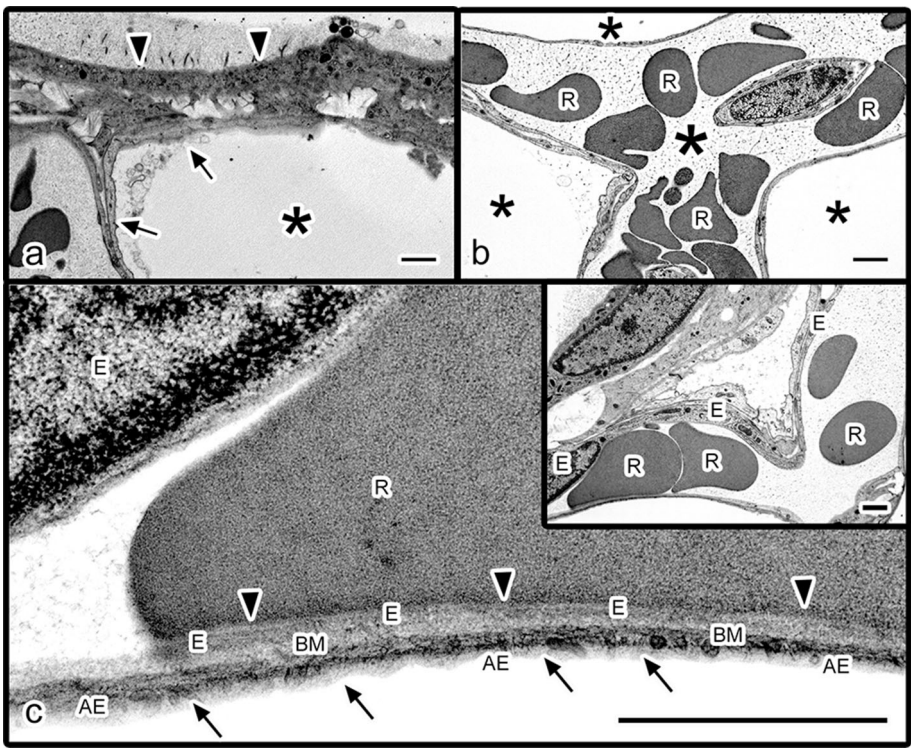

Fig. 7a–c Electron micrographs of the pleural and pulmonary structures of the inflated lungs of living mice obtained using the IVCT. **a** An electron micrograph of a mesothelial cell (*arrowheads*) and an alveolar septum (*arrows*) is shown. *Asterisk* pulmonary alveolus. **b** In another alveolar region, pulmonary alveoli (*small asterisks*) and blood capillaries (*large asterisk*) were closely associated with each other. *R* erythrocytes. **c** In the septal blood capillaries, flowing erythrocytes (*R*, *inset*) exhibited various shapes other than the typical biconcave discoid shape, and some erythrocytes adhered firmly to endothelial cells (*arrowheads*). *AE* alveolar type I epithelial cell, *BM* basement membrane, *E* endothelium. *Bars* 1 μm

appearance during respiration. Moreover, the intercellular events that occur during gas/material exchange have not been examined in such studies, and conventional electron microscopy has provided little information about the functional morphology of living animal lungs (Bastacky et al. 1995). Therefore, the IVCT was applied to morphological analyses of mouse lungs that were inflated using mechanical ventilation (Takayama et al. 2000). In the latter study, we examined the in vivo ultrastructures of the pulmonary epithelium and endothelium and circulating erythrocytes in living mouse lungs during respiration, as reported previously (Takayama et al. 2000).

Preparation procedures for living mouse lungs

Male mice weighing 20–30 g were anesthetized with sodium pentobarbital. Then, a 23-gauge cannula was inserted into the trachea and sutured in place. The mice were allowed to breathe spontaneously. The abdominal cavity and diaphragm were then opened, and mechanical ventilation with air was immediately initiated. At the moment of pulmonary distension, the whole lung was quickly frozen with a liquid IP mixture (−193 °C) that had been cooled with liquid nitrogen. The mouse itself was then placed in liquid nitrogen, and the well-frozen parts of the lungs were trimmed off with clippers in liquid nitrogen, as reported previously (Ohno et al. 1996). The specimens were then processed for FS, as described above. Next, they were briefly washed in pure acetone at room temperature and embedded in Quetol 812. After routine polymerization, ultrathin sections were prepared, contrast-stained with uranyl acetate and lead citrate, and examined with a Hitachi H-600 electron microscope.

New findings regarding the ultrastructures of the dynamically changing lungs

The functional structures of the pleura and subpleural regions of the mouse lung, including inflated alveoli, interstitial and alveolar epithelial cells, and the erythrocytes flowing through blood vessels, were well preserved in the ultrathin sections, and no marked ice crystal damage was seen (Fig. 7a). Moreover, the pulmonary alveoli and the blood capillaries containing flowing erythrocytes were found to be closely associated during electron microscopic examinations (Fig. 7b). The flowing erythrocytes exhibited various shapes other than the typical biconcave discoid form of such cells, as has been seen in other organs (Terada et al. 1998b; Xue et al. 2001). Some of them were partially attached to endothelial cells (Fig. 7c), indicating that such erythrocyte–endothelium attachment might be involved in the physiological functions responsible for gas exchange.

In the abovementioned study, we also examined the behavior of erythrocytes in blood capillaries within the alveolar septum. As a result, we demonstrated the ultrastructure of circulating erythrocytes and clarified their

morphology. The cells displayed various shapes, including no typical biconcave discoid shape. In previous studies, we obtained similar findings about the ultrastructures of circulating erythrocytes in other organs (Terada et al. 1998b; Xue et al. 1998, 2001). Erythrocytes and endothelial cells were often found in close proximity to each other in the peripheral regions of the pulmonary alveoli. This finding might reflect the intercellular communication that occurs during gas/material exchange through the very narrow basement membrane (Groniowski and Biczysko 1964; Voccaro and Brody 1981). In conclusion, the IVCT is useful for demonstrating the functional ultrastructures of living alveolar and pleural cells, which cannot be investigated using conventional electron microscopy preparation methods.

Smooth muscle cells in dystrophin-deficient mdx mice

Dystrophin, the product of the Duchenne muscular dystrophy (DMD) gene, is present in all types of muscle in normal individuals (Carlson 1998). In humans, the absence of dystrophin or the presence of an incomplete version of the protein is responsible for the development of DMD. Dystrophic mdx mice also lack dystrophin due to an X-linked mutation (Sicinski et al. 1989). DMD patients exhibit extensive and progressive skeletal muscle necrosis in their striated muscles and can develop life-threatening dilated cardiomyopathy (Carlson 1998). Under normal conditions, the dystrophin expression seen in smooth muscle cells is similar to that observed in striated muscle, but the smooth muscle cells of DMD patients do not express dystrophin (Harricane et al. 1991; Marbini et al. 1995, 1996). Dystrophin usually binds to the filamentous actin cytoskeleton and is normally found in a complex of transmembrane proteins that interact with the external components of the basal lamina (Byers et al. 1991; Brown 1997). This complex forms a structural bridge between the external basal lamina and the internal cytoskeleton, and the absence of dystrophin produces a defect in the structural support provided to the cell membrane which renders skeletal muscle susceptible to cell membrane rupture during the course of contractile activity (Carlson 1998). In fact, it was reported that normal myotubes were about fourfold stiffer than those cultured from mdx mice (Pasternak et al. 1995).

In smooth muscle, the basal lamina, which is considered to be constituted of intramuscular microtendons, plays a mechanical role in the transmission of force, and the abovementioned complex contributes to this activity (Gabella 1981). On the other hand, the membranes of smooth muscle cells display two alternating structural domains at the electron microscopic level: (1) densely stained plaques that correspond to the adherens junctions and (2) intervening uncoated regions, which are rich in invaginated caveolae (North et al. 1993). The bipartite domain structure of smooth muscle cell membranes contrasts with the more complex cell membrane arrangement seen in skeletal muscle. A number of molecules, including caveolin, Ca^{2+}-ATPase, and an inositol trisphosphate receptor-like protein, have been reported to localize in caveolae (Okamoto et al. 1998), which suggests that caveolae are involved in a diverse range of cytoplasmic processes, such as signal transduction. Dystrophin also specifically localizes in the caveolae-rich domains of smooth muscle cell membranes, together with caveolin (North et al. 1993; Okamoto et al. 1998). The purpose of this section is to describe the ultrastructural pathological changes that were detected in the smooth muscle cells of mdx mice in our IVCT-based study (Ohno et al. 1996).

Contracting muscle cells of scn or mdx mice

The intestinal organs of normal scn mice or dystrophin-deficient mdx mice were surgically exposed under pentobarbital anesthesia and put on a thin plastic plate. The IVCT was performed as described previously (Ohno et al. 1996). Some of the frozen specimens were routinely freeze-substituted in acetone containing 2 % osmium tetroxide and then embedded in epoxy resin. Ultrathin sections were cut, stained with uranium acetate and lead citrate, and examined with transmission electron microscopy. In the specimens from living scn mice, the smooth muscle cells in the outer muscle layers of the intestines were located close to each other, and they often spontaneously contracted in areas of the cytoplasm that contained caveolar structures (Fig. 8a). In the mdx mice, irregularly shaped caveolae and the fusion of several caveolae were seen more often than in the normal mice (Fig. 8b, inset). In addition, the intercellular spaces between the smooth muscle cells were more dilated (Fig. 8b), and the extracellular matrices were partially disrupted during muscle contraction (Fig. 8b).

Based on these findings, it was suggested that dystrophin deficiency impairs the development of normal cell morphology in both striated and smooth muscles. In dystrophic mammals, the histopathological changes that occur in smooth muscle cells have been examined in less detail than those seen in striated muscles (Marbini et al. 1995, 1996). In the latter studies, no smooth muscle cells that exhibited the typical findings of necrosis or apoptosis were identified among the thousands of examined mdx mouse muscle cells. It is unclear why most smooth muscle cells are able to survive in the absence of normal dystrophin expression, but there are several possible explanations. An elevated free cytosolic Ca^{2+} concentration, a potential trigger of cell necrosis, was

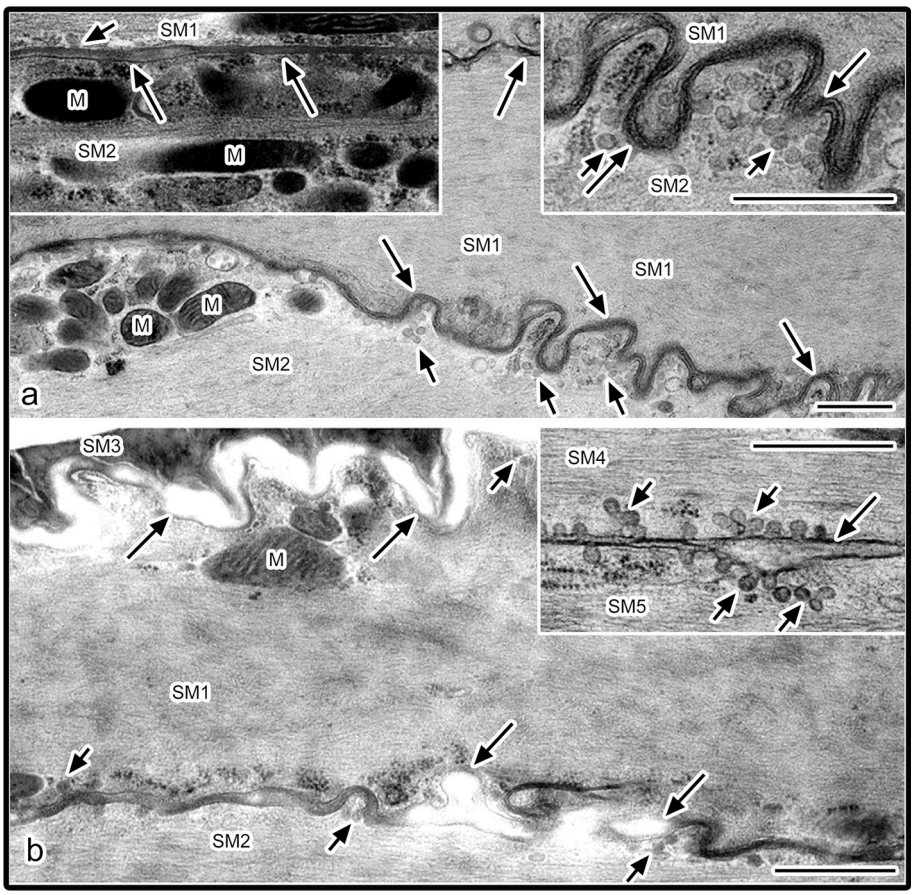

Fig. 8a–b Electron micrographs of intestinal smooth muscle cells from normal scn mice (**a**) or dystrophin-deficient mdx mice (**b**) prepared using the IVCT. **a** The intercellular matrix tightly adhered to the contracting smooth muscle cells (*SM1*, *SM2*) in the normal scn mice (*large arrows*). *Right upper inset* higher magnification; *left upper inset* non-contracting smooth muscle cells; *small arrows* caveolae, *M* mitochondria. **b** The intercellular spaces between the contracting smooth muscle cells were wider in the dystrophin-deficient mdx mice (*large arrows*) than in the normal scn mice. *SM1–SM5* smooth muscle cells; *inset* irregularly shaped or fused caveolae seen in the smooth muscle cells of the mdx mice (*small arrows*); *M* mitochondria, *small arrows* caveolae; *bars* 0.5 μm

detected in the skeletal muscle of mdx mice (McCarter et al. 1997). However, the cytosolic Ca^{2+} concentrations of the resting smooth muscle cells of mdx mice, which were measured with the fluorescent Ca^{2+} indicator fura-2, were normal (Boland et al. 1993). The maintenance of intracellular Ca^{2+} metabolism might contribute to smooth muscle cell homeostasis in mdx mice (Khurana et al. 1995).

Significance of the IVCT for examinations of functioning smooth muscles

We have previously noticed that ultrastructural tissue sections obtained using conventional preparation methods include numerous artifacts. In other words, the "normal" ultrastructures obtained using the standard methods are not natural. Indeed, the ultrastructural features exhibited by conventionally prepared sections of the smooth muscle cells of normal scn mice differ from those displayed by sections of the same tissue obtained using the IVCT. In IVCT-based examinations of scn mice, a very compact extracellular matrix was noted between the closely spaced smooth muscle cells. In contrast, disruptive changes were seen in the basement membranes of the mdx mice after the IVCT. The extracellular matrix and basal lamina have been suggested to contain intramuscular microtendons that provide mechanical support during contractions of the smooth muscle layer. In normal scn mice, the extracellular matrix contained tightly packed smooth muscle cells, and the intramembrane protein dystrophin was shown to play a role in connecting the extracellular matrix to the cell membranes of smooth muscle cells. However, the extracellular matrix was easily torn away from the smooth muscle cells in the mdx mice because of the functional impairment of dystrophin, which resulted in less compact smooth muscle layers. Such impairment could affect force transmission within the extracellular matrix and might decrease the force generated during the contraction of the smooth muscle layers (Gabella 1981). Thus, the IVCT has revealed the morphological features of spontaneously contracting smooth muscle cells in normal living mice and demonstrated that the extracellular matrix and caveolar features of such mice differ from those of dystrophin-deficient mdx mice.

Immunoelectron microscopy of dynamic cell organelles

The preparation of samples for post-embedding immunoelectron microscopy (immuno-EM) is affected by two main

problems. First, morphological alterations can be induced by anoxia or ischemia during specimen preparation. Second, in comparison with the strong contrast exhibited by ultrastructures in epoxy resin, hydrophilic resin obscures the ultrastructures of fixed specimens. However, the QF-DE method has been successfully used to clarify the three-dimensional molecular structures of the cells and tissues in immunolabeled specimens. This method is able to clearly demonstrate the three-dimensional localization of proteins in cells and tissues, although morphological artifacts remain a problem. On the other hand, some kinds of cell organelles, such as caveolae, are considered to be dynamic components with in vivo ultrastructures that can change very rapidly (Takayama et al. 1994, 1995; Anderson 1993; Michel 1998), and so conventional immuno-EM has technical limitations that reduce its utility for morphofunctional examinations of cells and tissues. The IVCT, which can be used to directly examine functioning cells or tissues in anesthetized animals, might help to solve such problems (Ohno et al. 1996). It has already provided new information about the ultrastructures of mouse glomerular capillary loops under various hemodynamic conditions (Ohno et al. 1996, 2001) and the erythrocytes flowing through hepatic sinusoids (Terada et al. 1998b). In a previous study, we combined the IVCT with the immuno-EM to clarify the in vivo localization of caveolin in functioning smooth muscle cells (Takayama et al. 1999).

Preparatory procedures for immuno-EM

In mice, the abdominal cavity was opened and the in vivo duodenum was examined with the naked eye. Then the serosal surface of the duodenal wall was immediately frozen in vivo using an IP mixture (−193 °C) that had been cooled in liquid nitrogen as a cryogen. The frozen duodenum was excised with a precooled nipper in liquid nitrogen (−196 °C), before being processed for DE. The serosal side of the duodenal tissue was carefully freeze-fractured with a scalpel in liquid nitrogen, as reported previously (Ohno et al. 1996, 2001). The tissue samples were then deeply etched under vacuum conditions of 6–8 $\times$ 10^{-5} Pa at −95 °C in an Eiko FD-3AS machine for 15–20 min. The specimens were placed on a cold stage and rotary shadowed with platinum and carbon. A drop of 2 % collodion in amyl acetate was added to the replicas as soon as the specimens were removed from the etching machine to prevent the replica membranes from breaking into pieces during the subsequent digestion procedure. The replicated specimens were coated with dried collodion and treated with 5 % sodium dodecyl sulfate in distilled water (pH 4.0) for 5–10 h, before being incubated with 0.5 % collagenase at 4 °C overnight. These treatments resulted in the retention of residual antigen proteins on the replica membranes. Then the replica membranes, together with the antigen proteins, were incubated with polyclonal rabbit anti-caveolin antibody, before being incubated with goat anti-rabbit IgG antibody conjugated with 10 nm gold. After the immunocytochemical procedures, the replica membranes were washed in phosphate-buffered saline and then cut into small pieces with a pair of scissors. Next, they were mounted on Formvar-filmed copper grids and immersed in amyl acetate solution to dissolve the collodion, before being examined with a Hitachi H-8100 electron microscope.

Immunolocalization of caveolin on replica membranes

As shown in Fig. 9a and b, our replica membrane method made it possible to examine the three-dimensional ultrastructures of smooth muscle cells in mouse duodenal samples that were prepared using the IVCT. Figure 9a shows the freeze-fractured cytoplasm of the smooth muscle cells of living mice, in which many three-dimensional cytoskeletons and cell organelles were seen. On the P-faces of the freeze-fractured cell membranes of the smooth muscle cells (Fig. 9b), caveolae were detected as small holes about 50–100 nm in diameter (when viewed from outside the cell). The diameters of the caveolae varied. Immunogold-labeled caveolin was often seen around these holes, which were probably attached to the caveolar walls (Fig. 9c). However, they were also found in some flat cell membrane regions in the smooth muscle cells of dystrophin-deficient mdx mice (Fig. 9d).

In this way, the use of the IVCT in combination with replica immuno-EM is useful for showing the native intracellular localization of caveolin in functioning smooth muscle cells. In addition, this technique can provide higher resolution images of replica membranes and allows us to examine the localization of caveolin around caveolae. Freeze-fracture replica immuno-EM has certain advantages for studies of the subcellular distribution of antigen proteins (Fujimoto 1995), but it has not been used to investigate animal organs under physiological conditions. Caveolae have been reported to contain various receptors and signaling molecules (Takayama et al. 1995; Anderson 1993) and to play important roles as cell membrane microdomains. In vivo ultrastructural examinations are required to reveal the dynamic processes involved in caveolae-based protein–protein interactions in living smooth muscle cells, which have barely been examined using conventional electron microscopic or immuno-EM methods. The IVCT can be used in combination with replica immuno-EM to directly examine living animal organs under various experimental conditions, which is an effective approach not only for morphofunctional investigations of caveolae (Takayama et al. 1999) but also for

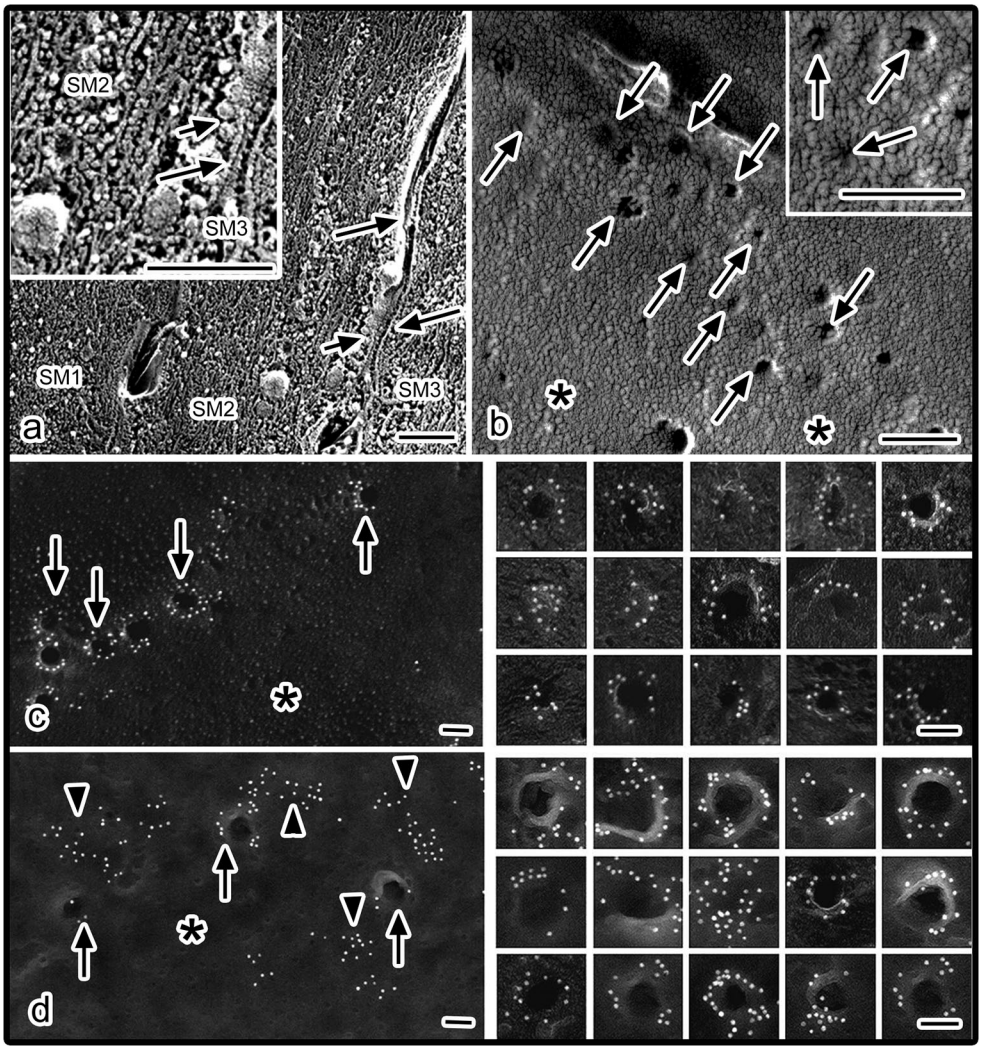

Fig. 9a–d Replica electron micrographs of the intestinal smooth muscle cells of living mice obtained using the IVCT followed by the replica membrane etching method. **a** The freeze-fractured cytoplasm of three parallel smooth muscle cells (*SM1–SM3*) is shown. The three-dimensional structures of many cytoskeletons and caveolar structures (*small arrows*) were seen along the sarcolemma (*large arrows*). *Inset* higher magnification; *bars* 0.5 µm. **b** Various types of caveolar neck structures (*arrows*) were observed on the freeze-fractured P-face of the sarcolemma (*asterisks*). *Right upper inset* higher magnification; *bars* 0.2 µm. **c**, **d** Replica immunoelectron-microscopic images of the distribution of caveolin in the smooth muscle cells of living scn (**c**) or mdx (**d**) mice. The *panels on the right* list the various caveolar structures that were labeled with immunogold particles. In the mdx mice (**d**), immunogold-labeled caveolin molecules were detected on both caveolae (*arrows*) and flat cell membranes (*arrowheads*). *Asterisks* freeze-fractured P-face; *bars* 0.1 µm

studies of the extracellular matrices of functioning organs (Zea-Aragon et al. 2004b).

Erythrocyte morphology under various blood flow conditions

Mammalian erythrocytes usually maintain their biconcave discoid shape in vitro, but their form changes frequently under the complex dynamic conditions found in blood vessels (Maeda 1996). However, little is known about the morphological appearance of the erythrocytes that flow through the blood vessels in various living animal organs because of the limitations of the conventional sample preparation techniques used for light or electron microscopy. It is also difficult to directly observe the behavior of erythrocytes as they flow through large blood vessels with thick walls or hepatic sinusoids in solid liver tissue. Therefore, conventional morphological studies based on the immersion- or perfusion-fixation method have not revealed the true functional morphology of circulating erythrocytes under various blood flow conditions. We used the IVCT to examine the behavior of flowing erythrocytes in living mouse structures, including large blood vessels and hepatic sinusoids. The abdominal aortae, inferior vena cavae, and livers of anesthetized mice were prepared using the IVCT, as described previously (Terada et al. 1998b; Xue et al. 1998). The frozen tissues were subjected to routine

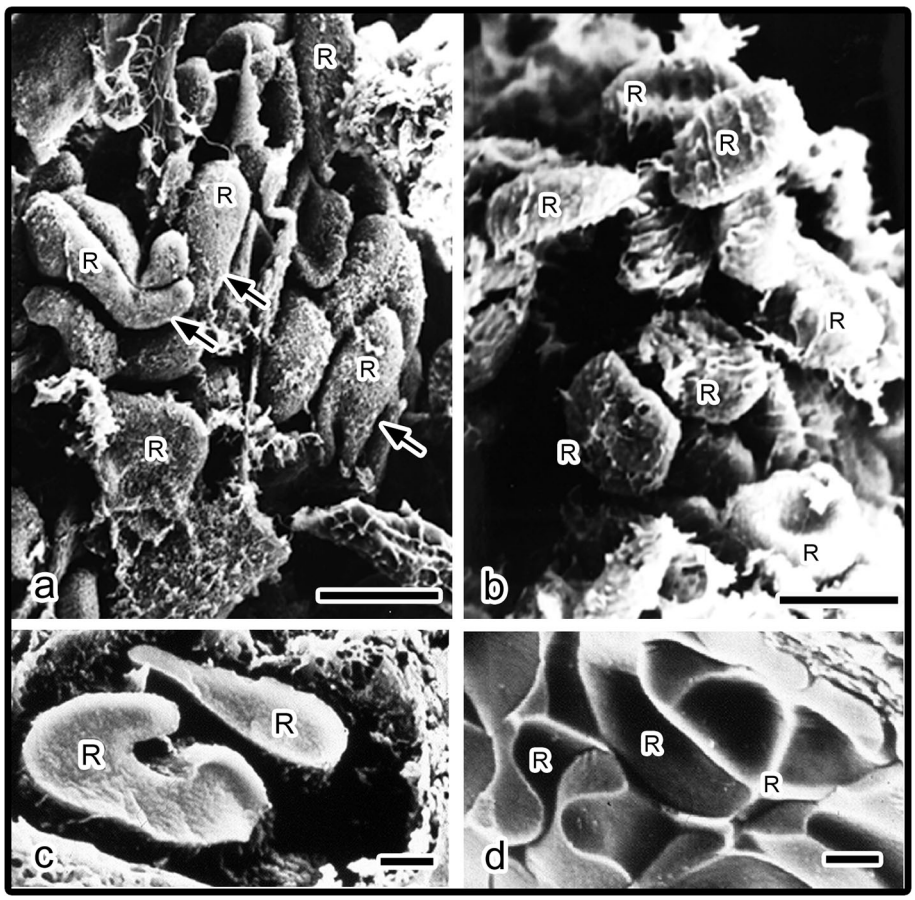

Fig. 10a–d Scanning electron micrographs of the erythrocytes flowing through the abdominal aortae (**a**), inferior vena cavae (**b**), and hepatic sinusoids of living mice under different blood flow conditions (**c**, **d**). All tissue samples were prepared using the IVCT. **a** The erythrocytes (*R*) flowing through the abdominal aorta exhibited various shapes, and some of them demonstrated ellipsoid forms (*arrows*). **b** Most of the erythrocytes in the inferior vena cava displayed the typical biconcave discoid shape. *Bars* 5 µm. **c**, **d** Scanning electron micrographs of the erythrocytes in the hepatic sinusoids of mice under normal blood flow (**c**) or cardiac arrest (**d**) conditions. The erythrocytes were prepared using the IVCT. **c** In the freeze-fractured sinusoids, flowing erythrocytes (*R*) of various shapes were seen. **d** Under cardiac arrest conditions, erythrocytes accumulated in the collapsed sinusoids, where they exhibited the typical biconcave discoid shape. *Bars* 1 µm

FS fixation and were examined using scanning electron microscopy.

Flowing erythrocytes in large blood vessels

The three-dimensional shapes of the flowing erythrocytes appeared to vary under the high-speed flow conditions found in the abdominal aorta, and some ellipsoid or curved erythrocytes were observed (Fig. 10a). On the other hand, most of the erythrocytes in the inferior vena cava, which were traveling at a lower speed, formed biconcave-discoid-like shapes (Fig. 10b). Previous studies have demonstrated that all of the erythrocytes in stored blood for human transfusions exhibit the typical biconcave discoid shape. However, those in large in vivo blood vessels are influenced by physiological rheology, which is affected by the bulk flow of the vessel (Stuart and Nash 1990). Arterial flow is usually laminar, especially in the abdominal aorta (Robinson 1978). Large arteries display high-velocity blood flow ($\sim$100 cm/s) and so are considered to be subject to a high shear rate (Klug et al. 1974). Thus, the erythrocyte deformation seen in such blood vessels might be caused by external forces. In our study, various erythrocyte shapes were seen in the aorta, with some erythrocytes being stretched in the direction of blood flow. Conversely, the low shear rate in the inferior vena cava, which flows at a velocity of 30 cm/s (Klug et al. 1974), resulted in erythrocytes with an approximately biconcave discoid shape.

In response to fluid shear forces, erythrocytes readily change from their resting biconcave discoid shape into an ellipsoid form, and their long axes align parallel to the fluid stream. Such temporary erythrocyte deformation in large blood vessels was clearly visible after the IVCT. It is tempting to conclude that the extent of erythrocyte deformation differs markedly between the abdominal aorta and

the inferior vena cava because venous blood exhibits significantly greater hematocrit values, plasma viscosity, and erythrocyte aggregation than arterial blood (Mokken et al. 1996). Therefore, the erythrocyte deformation seen in blood vessels might be dependent on the blood flow conditions and the functions of such cells in oxygen delivery. It is apparent that the shape and elasticity of flowing erythrocytes play important roles in the etiology of certain pathological conditions (Athanassiou et al. 1992; Cynober et al. 1996). For example, some types of hemolytic anemia are closely associated with increased mechanical fragility in erythrocyte membranes (Rybicki et al. 1993), which will be confirmed in vivo using the IVCT.

Shapes of the erythrocytes in the hepatic sinusoids of living mice

We have also used the IVCT to examine the shapes of the erythrocytes flowing through the hepatic sinusoids of living mice (Fig. 10c), as reported previously (Terada et al. 1998b). The morphological features of these cells differed from those of the erythrocytes flowing through the abdominal aorta and inferior vena cava, as described above. Wide spaces between flowing erythrocytes, which exhibited various shapes, were frequently observed in the hepatic sinusoids together with dilated spaces of Disse (Fig. 10c). However, after the artificial induction of cardiac arrest, erythrocytes accumulated in the sinusoidal lumen (Fig. 10d). In addition, the shapes of the erythrocytes observed in the mice subjected to cardiac arrest were completely different from those of the erythrocytes found in the hepatic sinusoids of living mice, and most of them appeared to have typical biconcave discoid shapes. Moreover, the hepatic sinusoids and spaces of Disse between hepatocytes and endothelial cells completely collapsed after cardiac arrest was induced. The flowing erythrocytes in the hepatic sinusoids exhibited persistent deformation, rather than returning to their typical biconcave discoid shapes, probably in response to hemodynamic stress. In isotonic physiological solution, erythrocytes generally display regular biconcave discoid shapes. The distance between the erythrocyte surface and the endothelium has physiological significance for the erythrocyte–capillary relationship; i.e., it affects the diffusion distance and shear stress. Moreover, while erythrocyte deformation allows erythrocytes to pass through narrow blood capillaries, it also increases the contact surface between the endothelium and erythrocytes, and effectively broadens the surface area for gas diffusion. Erythrocyte deformation and the surface structure of erythrocytes, including the membrane-skeletal proteins located under erythrocyte lipid membranes, are responsible for the constant flow of erythrocytes through narrow blood vessels (Shiga et al. 1990; Terada et al. 1997).

Elemental analysis of the erythrocytes in hepatic sinusoids

The IVCT was developed as a method for examining the shapes of the erythrocytes flowing through the large blood vessels and hepatic sinusoids of living mice, as described above (Terada et al. 1998b; Xue et al. 1998). However, there have not been any reports about the in vivo electrolyte concentrations of erythrocytes under various blood flow conditions. In the past few decades, variable-pressure scanning electron microscopy has often been used to examine hydrated and uncoated biological specimens. In the present study, we used the IVCT combined with the common freeze-drying method to prepare samples for examinations of the morphology of uncoated erythrocytes and the electrolyte levels of sinusoidal erythrocytes under normal blood flow conditions or after cardiac arrest, which were performed using a variable-pressure scanning electron microscope equipped with an X-ray microanalysis system.

The mice were anesthetized with sodium pentobarbital, and their livers were routinely prepared using the IVCT, as described previously (Terada et al. 1998b). The frozen liver surface was routinely freeze-fractured with a cryoknife in liquid nitrogen. The specimens were then freeze-dried at −95 °C in a freeze-etching apparatus (10^{-5} Pa) for 24 h, as reported previously (Yoshimura et al. 1991; Ohno et al. 1992). The freeze-dried specimens were gradually warmed up to room temperature. They were then attached to carbon plates using graphite-containing resin, and some of them were coated with carbon alone. Finally, they were analyzed using a Hitachi S-4300 scanning electron microscope or an S-3000 N variable-pressure scanning electron microscope equipped with an X-ray microanalysis system (accelerating voltage: 10 kV, vacuum pressure: 30 Pa, illumination current: 50 μA, analytical time: 950 s), or a conventional S-4500 scanning electron microscope (Hitachi High-Technologies Corporation, Tokyo, Japan) at an accelerating voltage of 10 kV. The following elements were analyzed: sodium (Na), phosphorus (P), sulfur (S), chloride (Cl), and potassium (K).

Figure 11a shows living mouse liver tissue that was freeze-fractured under normal blood flow conditions before being examined with a variable-pressure scanning electron microscope. Three-dimensional images of the hepatocytes of living mice and the erythrocytes (which exhibited various shapes) flowing through the hepatic sinusoids were easily detected without any metal coating. Small faint oval cellular organelles were seen in the cytoplasm of the hepatocytes. X-ray microanalysis of the flowing erythrocytes was performed under normal blood flow conditions (Fig. 11b). Potassium produced the highest peak, and sodium produced the lowest peak. Figure 11c shows freeze-fractured mouse liver tissue that was obtained after the induction of cardiac arrest. Erythrocytes with biconcave

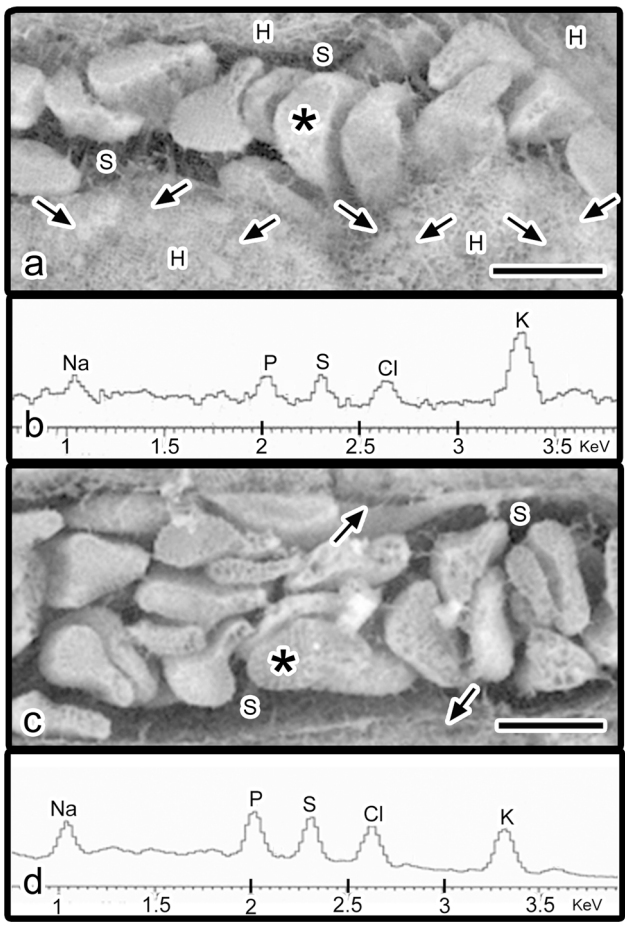

Fig. 11a–d Scanning electron micrographs of the hepatic sinusoids of living mice and X-ray microanalysis data for the detected erythrocytes. **a** Scanning electron micrographs of the freeze-fractured hepatic sinusoids of living mice obtained under normal blood flow conditions using a variable-pressure scanning electron microscope are shown. Images of liver tissue without any metal coating were obtained with backscattered electron beams. Flowing erythrocytes with various shapes were observed in the hepatic sinusoids (*S*). Freeze-fractured hepatocytes (*H*) were also noted, and some cell organelles were detected in their cytoplasm (*arrows*). *Bar* 5 μm. **b** The X-ray microanalysis data obtained for flowing erythrocytes (*asterisk*) under normal blood flow conditions are shown. The potassium peak (*K*) was the highest and the sodium peak (*Na*) was the lowest. **c** In the hepatic sinusoids (*S*) of the mice in which cardiac arrest was induced, the erythrocytes adhered to each other, but spaces of Disse were still observed (*arrows*). *Bar* 5 μm. **d** The X-ray microanalysis data for the erythrocytes (*asterisk*) in the liver of a mouse that was subjected to cardiac arrest are shown. The potassium peak (*K*) is clearly smaller than that seen in the normal blood flow conditions, whereas the sodium peak (*Na*) is larger

discoid shapes accumulated in the sinusoidal spaces because blood flow had ceased. In addition, some spaces of Disse were observed. The erythrocyte samples obtained after the induction of cardiac arrest were subjected to X-ray microanalysis (Fig. 11d). The potassium peak was lower than that seen in the normal conditions, but the sodium peak was slightly higher, probably because of anoxia. The peaks for phosphorus, sulfur, and chloride were similar under both conditions (Fig. 11b, d).

Thus, the elemental composition of the erythrocytes flowing through the hepatic sinusoids of mouse livers has been clarified under different hemodynamic conditions using variable-pressure scanning electron microscopy and X-ray microanalysis. Performing the IVCT in combination with variable-pressure scanning electron microscopy is a powerful tool for analyzing biological samples, and produces fewer technical artifacts associated with the diffusion or extraction of atomic elements from cells and tissues. In the erythrocytes flowing through the hepatic sinusoids of living mice, certain microenvironmental conditions might cause dynamic functional changes in the ion transport systems present in the cells' membranes, which are also affected by morphological changes.

New IVCT-based approaches for biomedical research

Measurement of erythrocyte oxygen saturation (SO_2) in blood vessels

The measurement of tissue oxygenation and erythrocyte SO_2 values is considered to be important for evaluating the state of living organs and intracellular responses to hypoxic conditions. Several analytical techniques have been used to examine regional differences in the oxygenation of cells and tissues in animals, including phosphorescence quenching, nuclear magnetic resonance spectroscopy, nicotinamide adenine dinucleotide fluorescence spectroscopy, and light or infrared spectroscopic and Raman imaging (Shelnutt et al. 1979; Wood et al. 2001; Nighswander-Rempel et al. 2002). One advantage of Raman microscopy for biological investigations is that the Raman spectrum of water is very weak, which is not the case in infrared spectroscopy (Cote 2001). This makes it possible to obtain precise information about the biological components of cells and tissues containing water and/or ice crystals. The recent development of a confocal Raman microscopy system has also aided the acquisition of such information from tiny target tissue samples within animal organ specimens, which in turn has made it possible to produce mapping images of their spectra (Terada et al. 2007a). The oxy- and deoxy-Hb-specific resonance Raman (RR) shifts of the blood vessels running through the abdominal peritoneum in living mice were recently examined using intravital Raman spectroscopic analyses (Torres Filho et al. 2005). However, the physiological relevance of low-temperature studies has not been elucidated in natural in vivo animal tissues (Ondrias et al. 1981). If specific RR shifts are also seen in living animal tissues at

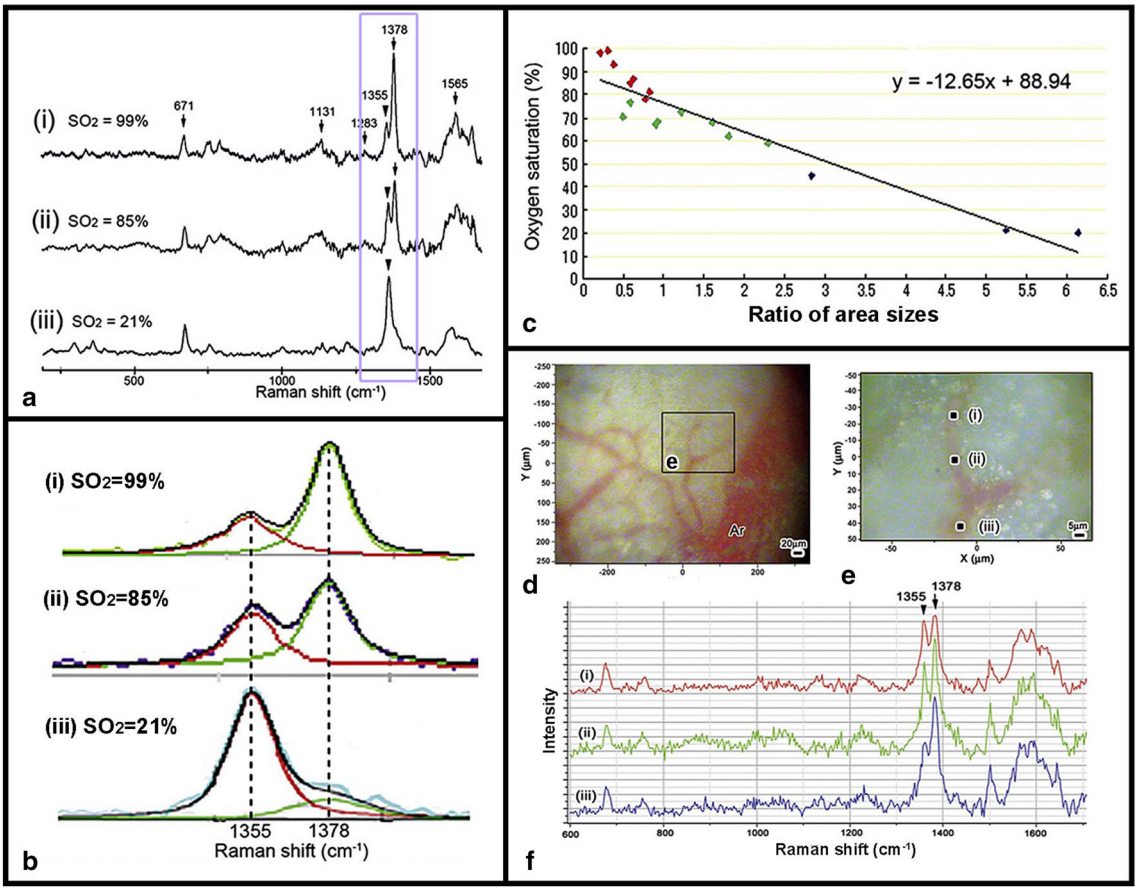

Fig. 12a–f The relationship between the Raman spectra of human whole blood and erythrocyte SO_2. **a**, **b** Raman spectra of human whole blood obtained at low temperature (−150 °C) under different oxygen saturation (SO_2) conditions. **c** A scatter plot demonstrating that erythrocyte SO_2 values were strongly correlated with the ratio of the areas of the shift peaks at 1355 and 1378 cm^{-1}. **d–f** In the small intestinal serous membranes of IVCT-prepared mice, three points were selected within the target blood vessels (*i–iii*) using a light microscope (**d**, **e**), and their Raman spectra were analyzed (**f**)

low temperature, the findings of Raman microscopic SO_2 analyses would probably reflect the functional living states of animal organs over millisecond-order periods. Therefore, human whole-blood samples that were obtained under various gas conditions from living mouse tissues that had been prepared with the IVCT were examined using confocal Raman microscopy at low temperature, which is referred to as "Raman cryomicroscopy" (Terada et al. 2008).

As a model for evaluating oxygen saturation using low-temperature Raman spectroscopy, the RR spectra of frozen human whole blood (HWB) were analyzed on a temperature-controllable stage at −150 °C with Raman microscopy. A 458-nm HeNe laser was focused on part of each frozen specimen on the cryostage with a bright-field microscope. Clear RR shift patterns were detected around 1355 and 1378 cm^{-1} (Fig. 12a, b). The 1378 and 1355 cm^{-1} Raman shift peaks changed with SO_2 (Fig. 12a, b). A scatter plot demonstrated that the erythrocyte SO_2 values and the ratios of the two shift peak areas were closely correlated with each other (Fig. 12c). Thus, the SO_2 of erythrocytes can be calculated by comparing the two RR shifts, as reported previously (Terada et al. 2008).

In our previous study, small intestines that had been prepared with the IVCT (Ohno et al. 1996) were analyzed with confocal Raman cryomicroscopy (Fig. 12d–f). Blood vessels were exposed by freeze-fracturing the surrounding tissue with a cooled scalpel (e in Fig. 12d). The intestinal mesentery and serous membrane contained many typical small arteries and veins (Fig. 12d, e). The peak shifts of the frozen intestinal tissues around 1355 and 1378 cm^{-1} completely matched the RR shifts of HWB (Fig. 12f), indicating that these values are a common characteristic of all animal hemoglobin molecules (Igarashi et al. 2003). Under a light microscope, some branches of the small arteries and arterioles exhibited a bright red color (Fig. 12d, e), and the Raman shifts of the blood vessels were analyzed with confocal Raman cryomicroscopy (Fig. 12f). In some arteries, the area

ratios of the two shift peaks gradually changed depending on the distance (in the peripheral direction) from a particular point of the target artery (Fig. 12f); i.e., the 1378 cm^{-1} Raman shift peak decreased relative to the 1355 cm^{-1} shift peak as the examined distance increased. Thus, the Raman spectra of frozen tissue samples that are obtained at low temperature can be used as an indicator of the SO_2 of flowing erythrocytes, as discussed in detail in previous studies (Terada et al. 2008).

Imaging of the microcirculation in the lungs of mice with metastatic melanoma

Metastatic cancer cells often induce hypercoagulable states, including platelet aggregation, which are strongly associated with the subsequent occurrence of processes linked to tumor progression, e.g., cell proliferation and angiogenesis (Hilgard 1973; Manegold et al. 2003; Holmes et al. 2009). In addition to platelet-related effects, some cancer cells were also demonstrated to produce coagulation factors, such as thrombin and tissue factors (Jurasz et al. 2004; Jain et al. 2010; Bambace and Holmes 2011). Clinically, cancer-induced hypercoagulable states often cause disseminated intravascular coagulation (DIC) in humans (Kvolik et al. 2010; Bambace and Holmes 2011). DIC is usually confirmed by the detection of reductions in the fibrinogen level and platelet count and/or increases in the concentrations of D-dimer, fibrinogen degradation products, and soluble fibrin monomers in blood and plasma tests (Munter and Hershko 2001). In particular, the level of soluble fibrin monomers is an indicator of initial blood coagulation because it is the first product of fibrinogen cleavage by thrombin (Budzynski et al. 1983). Soluble fibrin monomers are also reported to enhance activated platelet adhesion to cancer cells, which was confirmed by an increase in the lung metastasis of cancer cells that had been pretreated with soluble fibrin (Biggerstaff et al. 1999). A monoclonal antibody that reacted with thrombin-cleaved fibrinogen was developed to detect soluble fibrin monomers in plasma in vitro (Hamano et al. 2002). However, as most of the soluble components and molecular structures in blood vessels are readily removed or changed during tissue preparation with conventional chemical fixation methods, we employed the IVCT to prepare tissue sections for microscopic analyses of such functional areas for evaluating the timing of initial thrombus formation, as reported previously (Saitoh et al. 2014).

To visualize thrombi, we injected mouse melanoma cells into the right ventricles of anesthetized mice. At 5 s after the injection of the melanoma cells, their entry into large pulmonary blood vessels and some alveolar capillaries was clearly detected (Fig. 13a). The blood vessels

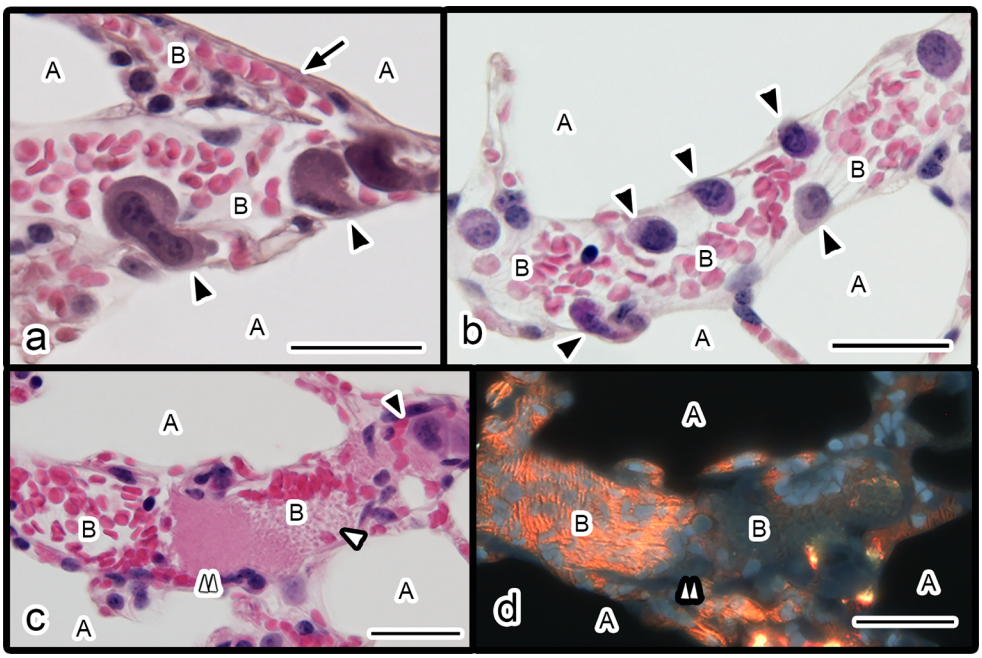

Fig. 13a–d Light micrographs of mouse lung tissues that were prepared using the IVCT at 5 s (**a**), 1 min (**b**), and 5 min (**c**, **d**) after the injection of melanoma cells into the right ventricle. Hematoxylin and eosin (*HE*)-stained morphological features (**a–c**) and the distributions of injected *quantum dots* (QD) (**d**) after the injection of melanoma cells are shown. An HE-stained image of a serial paraffin section is shown (**c**). A QD-fluorescence image (obtained using ultraviolet light) of a tissue section containing *red-colored* blood vessels (**d**) is shown. *Black arrow* visceral pleura, *black arrowheads* melanoma cells, *white arrowhead* platelets, *white double arrowheads* large platelet aggregates, *B* blood vessel, *A* alveolus; *bars* 25 μm (color figure online)

were filled with numerous erythrocytes. At 1 min, some melanoma cells had adhered to the endothelial walls of the large blood vessels (Fig. 13b). At this stage, fluorescent quantum dots (QD), which had been injected into the right ventricle to examine blood circulation (Terada et al. 2010; Saitoh et al. 2012), were detected in all of the examined blood vessels. At 5 min after the injection of the melanoma cells, many platelets had accumulated and aggregated in the larger blood vessels (Fig. 13c). Initial thrombus formation, usually accompanied by melanoma cell metastasis, was visualized in HE-stained paraffin sections obtained using the IVCT, which accurately reflected the living state of mouse lungs. The QD were rarely detected in the blood vessels that contained large platelet aggregates (Fig. 13d). These findings suggest that the IVCT is able to reveal the initial morphological effects of thrombus formation, which is sometimes accompanied by the subsequent failure of blood circulation, as discussed previously in detail (Saitoh et al. 2014).

Recently, clear images of cancer cell invasion and proliferation in living animals have been obtained using intravital imaging techniques (Condeelis and Seqall 2003; Winkler et al. 2009). Therefore, combining current bioimaging techniques with the IVCT could be useful for obtaining accurate information about the mechanisms responsible for thrombosis and hemostasis in living animal tissues. It is considered that the temporary adhesion of cancer cells to blood vessel walls usually occurs within a couple of seconds, as revealed by a live-imaging technique (Gassmann et al. 2010). In a previous study, we observed histological events, such as the intrusion and stacking of melanoma cells in blood vessels, which probably reflected the temporary attachment of such cells to blood vessel walls, within 5 s of the injection of the melanoma cells. In another report concerning the stable adhesion of cancer cells to vascular walls, it was found that colon cancer cells took more than 10 s to adhere to blood vessel walls (Gassmann et al. 2010). In a previous study, we detected the stacking and attachment of melanoma cells within blood vessels at 1 min after their injection. Therefore, it would be very useful to compare these findings with those revealed using live-imaging techniques (Saitoh et al. 2014).

Concluding remarks

Many molecular components and structures of living animal or human organs undergo dynamic changes as part of their functions, and these processes occur within extracellular or intracellular fluid. The importance of cryofixation for morphological and immunohistochemical examinations, as described in this review, is based on the way the water in tissues and cells forms tiny vitreous ice crystals. Our ultimate goal as morphological scientists is to obtain accurate information about the histology and pathology of living animal (including human) organs and the localization of functional molecules in cells and tissues. The IVCT presented in this review is a first step to being able to instantly stop the normal blood circulation of living animals before performing light- or electron-microscopic examinations. It is now possible to perform direct morphological and immunohistochemical analyses of living animal organs using the IVCT without causing major ischemia or anoxia. We have already used this technique to obtain various novel cell and tissue findings that have never been seen in studies using other conventional preparation methods. As the IVCT makes it possible to obtain functional morphological findings that are closer to the actual state of living animal organs than those produced using conventional preparation methods, it will surely lead to the development of "living animal morphology" as a new morphological field, which would complement the dynamic images obtained using novel live-imaging methods. In the future, we predict that there will be a morphological renaissance in which many discoveries about living animal or human organs will be made.

Compliance with ethical standards

Conflict of interest None.

References

Anderson RGW (1993) Caveolae: where incoming and outgoing messengers meet. Proc Natl Acad Sci USA 90:10909–10913

Andrews P (1988) Morphological alterations of the glomerular (visceral) epithelium in response to pathological and experimental situations. J Electron Microsc Tech 9:115–144

Athanassiou G, Symeonidis A, Kourakli A, Missirlis YF, Zoumbos NC (1992) Deformability of the erythrocyte membrane in patients with myelodysplastic syndromes. Acta Haematol 87:169–172

Bambace NM, Holmes CE (2011) The platelet contribution to cancer progression. J Thromb Haemost 9:237–249

Bastacky J, Lee CY, Goerke J, Koushafar H, Yager D, Kenaga L, Speed TP, Chen Y, Clements JA (1995) Alveolar lining layer is thin and continuous: low-temperature scanning electron microscopy of rat lung. J Appl Physiol 79:1615–1628

Biggerstaff JP, Seth N, Amirkhosravi A, Amaya M, Fogarty S, Meyer TV, Siddiqui F, Francis JL (1999) Soluble fibrin augments platelet/tumor cell adherence in vitro and in vivo, and enhances experimental metastasis. Clin Exp Metastasis 17:723–730

Bohrer MP, Deen WM, Robertson CR, Brenner BM (1977) Mechanism of angiotensin II-induced proteinuria in the rat. Am J Physiol 233:F13–F21

Boland B, Himpens B, Casteels R, Gillis JM (1993) Lack of dystrophin but normal calcium homeostasis in smooth muscle from dystrophic mdx mice. J Muscle Res Cell Motil 14:133–139

Brenner BM, Bohner MP, Baylis C, Deen WM (1977) Determinants of glomerular permselectivity: insights derived from observations in vivo. Kidney Int 12:229–237

Brown RH Jr (1997) Dystrophin-associated proteins and the muscular dystrophies. Annu Rev Med 48:457–466

Budzynski AZ, Olexa SA, Pandya BV (1983) Fibrin polymerization sites in fibrinogen and fibrin fragments. Ann N Y Acad Sci 408:301–314

Byers TJ, Kunkel LM, Watkins SC (1991) The subcellular distribution of dystrophin in mouse skeletal, cardiac, and smooth muscle. J Cell Biol 115:411–421

Carlson CG (1998) The dystrophinopathies: an alternative to the structural hypothesis. Neurobiol Dis 5:3–15

Cole R, Matuszek G, See C, Rieder CL (1990) A simple pneumatic device for plunge-freezing cells grown on electron microscopy grids. J Electron Microsc Tech 16:167–173

Condeelis J, Seqall JE (2003) Intravital imaging of cell movement in tumours. Nat Rev Cancer 3:921–930

Cote GL (2001) Noninvasive and minimally-invasive optical monitoring technologies. J Nutr 131:1596–1604

Cynober T, Mohandas N, Tchernia G (1996) Red cell abnormalities in hereditary spherocytosis: relevance to diagnosis and understanding of the variable expression of clinical severity. J Lab Clin Med 128:259–269

Drumond MC, Deen WM (1994) Structural determinants of glomerular hydraulic permeability. Am J Physiol 266:F1–F12

Fujimoto K (1995) Freeze-fracture replica electron microscopy combined with SDS digestion for cytochemical labeling of integral membrane proteins—application to the immunogold labeling of intercellular junctional complexes. J Cell Sci 108:3443–3450

Furukawa T, Ohno S, Oguchi H, Hora K, Tokunaga S, Furuta S (1991) Morphometric study of glomerular slit diaphragms fixed by rapid-freezing and freeze-substitution. Kidney Int 40:621–624

Gabella G (1981) Structure of smooth muscle. In: Buelbring E, Brading AF, Jones AW, Tomita T (eds) An assessment of current knowledge. University of Texas Press, Austin, pp 1–46

Gassmann P, Kang ML, Mees ST, Haier J (2010) In vivo tumor cell adhesion in the pulmonary microvasculature is exclusively mediated by tumor cell–endothelial cell interaction. BMC Cancer 10:177

Griffith LD, Bulger RE, Trump BF (1967) The ultrastructure of the functioning kidney. Lab Investig 16:220–246

Groniowski J, Biczysko W (1964) Regulation of transport across pulmonary alveolar epithelial cell monolayers. Nature 204:745–747

Ham AW, Cormack DH (1978) Histology, 8th edn. JB Lippincott, Philadelphia

Hamano A, Tanaka S, Takeda Y, Umeda M, Sakata Y (2002) A novel monoclonal antibody to fibrin monomer and soluble fibrin for the detection of soluble fibrin in plasma. Clin Chim Acta 318:25–32

Harreveld AV, Crowell J (1964) Electron microscopy after rapid freezing on a metal surface and substitution fixation. Anat Rec 149:381–386

Harricane MC, Augier N, Leger J, Anoal M, Cavadore C, Mornet D (1991) Ultrastructural localization of dystrophin in chicken smooth muscle. Cell Biol Intern Rep 15:687–697

Hilgard P (1973) The role of blood platelets in experimental metastases. Br J Cancer 28:429–435

Holmes CE, Levis JE, Ornstein DL (2009) Activated platelets enhance ovarian cancer cell invasion in a cellular model of metastasis. Clin Exp Metastasis 26:653–661

Igarashi J, Sato A, Kitagawa T, Sagami I, Shimizu T (2003) CO binding study of mouse heme-regulated eIF-2a kinase: kinetics and resonance Raman spectra. Biochim Biophys Acta 1650:99–104

Jain S, Harris J, Ware J (2010) Platelets: linking hemostasis and cancer. Arterioscler Thromb Vasc Biol 30:2362–2367

Jehl B, Bauer R, Dorge A, Rick R (1981) The use of propane/isopentane mixtures for rapid freezing of biological specimens. J Microsc 123:307–309

Jurasz P, Alonso-Escolano D, Radomski MW (2004) Platelet–cancer interactions: mechanisms and pharmacology of tumour cell induced platelet aggregation. Br J Pharmacol 143:819–826

Kanwar YS (1984) Biophysiology of glomerular filtration and proteinuria. Lab Investig 51:7–21

Khurana TS, Prendergast RA, Alameddine HS, Tomé FM, Fardeau M, Arahata K, Sugita H, Kunkel LM (1995) Absence of extraocular muscle pathology in Duchenne's muscular dystrophy: role for calcium homeostasis in extraocular muscle sparing. J Exp Med 182:467–475

Klug PP, Lessin LS, Radice P (1974) Rheological aspects of sickle cell disease. Arch Int Med 133:577–590

Kriz W, Hackenthal E, Nobiling R, Sakai T, Elger M (1994) A role for podocytes to counteract capillary wall distension. Kidney Int 45:369–376

Kvolik S, Jukic M, Matijevic M, Marjanovic K, Glavas-Obrovac L (2010) An overview of coagulation disorders in cancer patients. Surg Oncol 19:e33–e46

Maeda N (1996) Erythrocyte rheology in microcirculation. Jpn J Physiol 46:1–14

Manegold PC, Hutter J, Pahernik SA, Messmer K, Dellian M (2003) Platelet–endothelial interaction in tumor angiogenesis and microcirculation. Blood 101:1970–1976

Marbini A, Marcello N, Bellanova MF, Guidetti D, Ferrari A, Gemignani F (1995) Dystrophin expression in skin biopsy immunohistochemical localisation of striated muscle type dystrophin. J Neurol Sci 129:29–33

Marbini A, Gemignani F, Bellanova MF, Guidetti D, Ferrari A (1996) Immunohistochemical localization of utrophin and other cytoskeletal proteins in skin smooth muscle in neuromuscular diseases. J Neurol Sci 143:156–160

McCarter GC, Denetclaw WFJ, Reddy P, Steinhardt RA (1997) Lipofection of a cDNA plasmid containing the dystrophin gene lowers intracellular free calcium and calcium leak channel activity in mdx myotubes. Gene Ther 4:483–487

Michel CC (1998) Capillaries, caveolae, calcium and cyclic nucleotides: a new look at microvascular permeability. J Mol Cell Cardiol 30:2541–2546

Mokken FC, Waart FJ, Henny CP, Goedhart PT, Gelb AW (1996) Differences in peripheral arterial and venous hemorheologic parameters. Ann Hematol 73:135–137

Moor H, Bellin G, Sandri C, Akert K (1980) The influence of high pressure freezing on mammalian nerve tissue. Cell Tissue Res 209:201–216

Munter G, Hershko C (2001) Increased warfarin sensitivity as an early manifestation of occult prostate cancer with chronic disseminated intravascular coagulation. Acta Haematol 105:97–99

Nighswander-Rempel SP, Anthony Shaw R, Mansfield JR, Hewko M, Kupriyanov VV, Mantsch HH (2002) Regional variations in myocardial tissue oxygenation mapped by near-infrared spectroscopic imaging. J Mol Cell Cardiol 34:1195–1203

North AJ, Galazkiewicz B, Byers TJ, Glenney JR Jr, Small JV (1993) Complementary distributions of vinculin and dystrophin define two distinct sarcolemma domains in smooth muscle. J Cell Biol 120:1159–1167

Ohno S, Hora K, Furukawa T, Oguchi H (1992) Ultrastructural study of the glomerular slit diaphragm in fresh unfixed kidneys by a quick-freezing method. Virchows Arch B Cell Pathol 61:351–358

Ohno S, Terada N, Fujii Y, Ueda H, Takayama I (1996) Dynamic structure of glomerular capillary loop as revealed by an in vivo cryotechnique. Virchows Arch 427:519–527

Ohno S, Kato Y, Xiang T, Terada N, Takayama I, Fujii Y, Baba T (2001) Ultrastructural study of mouse renal glomeruli under various hemodynamic conditions by an "in vivo cryotechnique". Ital J Anat Embryol 106:431–438

Ohno N, Terada N, Fujii Y, Baba T, Ohno S (2004) "In vivo cryotechnique" for paradigm shift to "living morphology" of animal organs. Biomed Rev 15:1–19

Ohno N, Terada N, Murata S, Katoh R, Ohno S (2005) Application of cryotechniques with freeze-substitution for the immunohistochemical demonstration of intranuclear pCREB and chromosome territory. J Histochem Cytochem 53:55–62

Ohno S, Ohno N, Terada N (eds) (2016) In vivo cryotechnique in biomedical research and application for bioimaging of living animal organs. Springer, Berlin

Okamoto T, Schlegel A, Scherer PE, Lisanti MP (1998) Caveolins, a family of scaffolding proteins for organizing "preassembled signaling complexes" at the plasma membrane. J Biol Chem 273:5419–5422

Olivetti G, Kithier K, Giacomelli F, Wiener J (1981) Glomerular permeability to endogenous proteins in the rat. Lab Investig 44:127–137

Ondrias MR, Rousseau DL, Simon SR (1981) Structural changes at the heme induced by freezing hemoglobin. Science 213:657–659

Pasternak C, Wong S, Elson EL (1995) Mechanical function of dystrophin in muscle cells. J Cell Biol 128:355–361

Plattner H, Bachmann L (1982) Cryofixation: a tool in biological ultrastructural research. Int Rev Cytol 79:237–304

Robinson K (1978) Abdominal aorta. In: James DG (ed) Circulation of the blood. Pitman Medical, Tunbridge Wells, pp 173–175

Ryan GB, Karnovsky MJ (1976) Distribution of endogenous albumin in the rat glomerulus: role of hemodynamic factors in glomerular barrier function. Kidney Int 9:36–45

Ryan GB, Hein SJ, Karnovsky MJ (1976) Glomerular permeability to proteins. Effects of hemodynamic factors on the distribution of endogenous immunoglobulin G and exogenous catalase in the rat glomerulus. Lab Investig 34:415–427

Rybicki AC, Qiu JJ, Musto S, Rosen NL, Nagel RL, Schwartz RS (1993) Human erythrocyte protein 4.2 deficiency associated with hemolytic anemia and a homozygous 40 glutamic acid-lysine substitution in the cytoplasmic domain of band 3. Blood 81:2155–2165

Saitoh Y, Terada N, Saitoh S, Ohno N, Jin T, Ohno S (2012) Histochemical analyses and quantum dot imaging of microvascular blood flow with pulmonary edema in living mouse lungs by "in vivo cryotechnique". Histochem Cell Biol 137:137–151

Saitoh Y, Terada N, Ohno N, Hamano A, Okumura N, Jin T, Saiki I, Ohno S (2014) Imaging of thrombosis and microcirculation in mouse lungs of initial melanoma metastasis with in vivo cryotechnique. Microvasc Res 91:73–83

Shelnutt JA, Rousseau DL, Friedman JM, Simon SR (1979) Protein–heme interaction in hemoglobin: evidence for Raman difference spectroscopy. Proc Natl Acad Sci USA 76:4409–4413

Shiga T, Maeda N, Kon K (1990) Erythrocyte rheology. Crit Rev Oncol Hematol 10:9–48

Sicinski P, Allan YG, Ryder-Cook AS, Barnard EA, Darlison MG, Barnard PJ (1989) The molecular basis of muscular dystrophy in the mdx mouse: a point mutation. Science 244:1578–1580

Stuart J, Nash GB (1990) Red cell deformability and haematological disorders. Blood Rev 4:141–147

Studer D, Michel M, Müller M (1989) High pressure freezing comes of age. Scanning Microsc Suppl 3:253–269

Takayama I, Fujii Y, Ohno S, Fujino MA (1994) Ultrastructural study of mast cells stimulated with compound 48/80 as revealed by quick-freezing method. Virchows Arch 424:287–294

Takayama I, Fujii Y, Ohno S, Fujino MA (1995) Freeze-fracture immunocytochemistry for intracellular localization of serotonin in rat mast cells stimulated with compound 48/80. Virchows Arch 426:267–270

Takayama I, Terada N, Baba T, Ueda H, Kato Y, Fujii Y, Ohno S (1999) "In vivo cryotechnique" in combination with replica immunoelectron microscopy for caveolin in smooth muscle cells. Histochem Cell Biol 112:443–445

Takayama I, Terada N, Baba T, Ueda H, Fujii Y, Kato Y, Ohno S (2000) Dynamic ultrastructure of mouse pulmonary alveoli revealed by an in vivo cryotechnique in combination with freeze-substitution. J Anat 197:199–205

Terada N, Ohno S (1998) Dynamic morphology of erythrocytes revealed by cryofixation technique. Acta Anat Nippon 73:587–593

Terada N, Ohno S (2004) Immunohistochemical application of cryotechniques to native morphology of cells and tissues. Acta Histochem Cytochem 37:339–345

Terada N, Fujii Y, Ueda H, Ohno S (1997) Immunocytochemical study of human erythrocyte membrane skeletons under stretching conditions by quick-freezing and deep-etching method. J Anat 190:397–404

Terada N, Fujii Y, Kato Y, Ueda H, Baba T, Ohno S (1998a) Scanning electron microscopic study of erythrocyte shapes artificially jetted through tubes at different pressures by 'in vitro cryotechnique for erythrocytes'. J Electron Microsc 47:489–493

Terada N, Kato Y, Fujii Y, Ueda H, Baba T, Ohno S (1998b) Scanning electron microscopic study of flowing erythrocytes in hepatic sinusoids as revealed by 'in vivo cryotechnique'. J Electron Microsc 47:67–72

Terada N, Banno Y, Ohno N, Fujii Y, Murate T, Sarna JR, Hawkes R, Zea Z, Baba T, Ohno S (2004) Compartmentation of the mouse cerebellar cortex by sphingosine kinase. J Comp Neurol 469:119–127

Terada N, Ohno N, Saitoh S, Fujii Y, Ohguro H, Ohno S (2007a) Raman microscopy of freeze-dried mouse eyeball-slice in conjunction with the "in vivo cryotechnique". Microsc Res Tech 70:634–639

Terada N, Ohno N, Saitoh S, Ohno S (2007b) Immunohistochemical detection of hypoxia in mouse liver tissues treated with pimonidazole using "in vivo cryotechnique". Histochem Cell Biol 128:253–261

Terada N, Ohno N, Saitoh S, Ohno S (2008) Application of "in vivo cryotechnique" to detect erythrocyte oxygen saturation in frozen mouse tissues with confocal Raman cryomicroscopy. J Struct Biol 163:147–154

Terada N, Saitoh Y, Saitoh S, Ohno N, Jin T, Ohno S (2010) Visualization of microvascular blood flow in mouse kidney and spleen by quantum dot injection with "in vivo cryotechnique". Microvasc Res 80:491–498

Torres Filho IP, Terner J, Pittman RN, Somera LG, Ward KR (2005) Hemoglobin oxygen saturation measurements using resonance Raman intravital microscopy. Am J Physiol Heart Circ Physiol 289:H488–H495

van Harreveld A, Trubatch J (1975) Synaptic changes in frog brain after stimulation with potassium chloride. J Neurocytol 4:33–46

Voccaro CA, Brody JS (1981) Structural features of alveolar wall basement membrane in the adult rat lung. J Cell Biol 91:427–437

Winkler F, Kienast Y, Fuhrmann M, Von Baumgarten L, Burgold S, Mitteregger G, Kretzschmar H, Herms J (2009) Imaging glioma cell invasion in vivo reveals mechanisms of dissemination and peritumoral angiogenesis. Glia 57:1306–1315

Wood BR, Tait B, McNaughton D (2001) Micro-Raman characterization of the R to T state transition of haemoglobin within a single living erythrocyte. Biochim Biophys Acta 1539:58–70

Xue M, Terada N, Fujii Y, Baba T, Ohno S (1998) Morphological study by an 'in vivo cryotechnique' of the shape of erythrocytes circulating in large blood vessels. J Anat 193:73–79

Xue M, Baba T, Terada N, Kato Y, Fujii Y, Ohno S (2001) Morphological study of erythrocyte shapes in red pulp of mouse spleens revealed by an in vivo cryotechnique. Histol Histopathol 16:123–129

Yoshimura A, Ohno S, Nakano K, Oniki H, Inui K, Ideura T, Koshikawa S (1991) Three-dimensional ultrastructure of anionic sites of the glomerular basement membrane by a quick-freezing and deep etching method using a cationic tracer. Histochemistry 96:107–113

Yu Y, Leng CG, Kato Y, Ohno S (1997) Ultrastructural study of glomerular capillary loops at different perfusion pressures as revealed by quick-freezing, freeze-substitution and conventional fixation methods. Nephron 76:452–459

Yu Y, Leng CG, Kato Y, Terada N, Fujii Y, Ohno S (1998) Ultrastructural study of anionic sites in glomerular basement membranes at different perfusion pressures by quick-freezing and deepetching method. Nephron 78:88–95

Zea-Aragon A, Terada N, Ohno N, Fujii Y, Baba T, Ohno S (2004a) Effects of anoxia on serum immunoglobulin and albumin leakage through blood–brain barrier in mouse cerebellum as revealed by cryotechniques. J Neurosci Methods 138:89–95

Zea-Aragon Z, Terada N, Ohno N, Fujii Y, Baba T, Yoshida M, Ohtsuki K, Ohnishi M, Ohno S (2004b) Replica immunoelectron microscopic study of the upper surface layer in rat mandibular condylar cartilage by a quick-freezing method. Histochem Cell Biol 121:255–259

Zhou H, Ohno N, Terada N, Saitoh S, Fujii Y, Ohno S (2007) Involvement of follicular basement membrane and vascular endothelium in blood–follicle barrier formation of mice revealed by 'in vivo cryotechnique'. Reproduction 134:307–317